Atmospheric Environment 315 (2023) 120140

Contents lists available at ScienceDirect

Atmospheric Environment

journal homepage: www.elsevier.com/locate/atmosenv

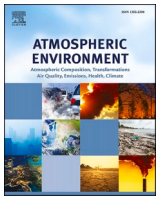

Concentration contextualisation, temporal patterns and sources of hydrogen sulphide at a site on the South African Highveld

E. Cogho [a], J.P. Beukes [a], P.G. van Zyl [a,*], V. Vakkari [a,b], L. Laakso [a,b], M. Josipovic [a], M. Kulmala [c]

[a] Atmospheric Chemistry Research Group, Chemical Resource Beneficiation, North-West University, Potchefstroom, ZA-2520, Potchefstroom, South Africa
[b] Finnish Meteorological Institute, FI-00101, Helsinki, Finland
[c] Institute for Atmospheric and Earth System Research, Physics, Faculty of Science, University of Helsinki Finland, PO Box 64 (Gustaf Hällströmin katu 2a), FI-00014, South Africa

HIGHLIGHTS

- A H_2S mean of 3.1 ppb was reported for a 2-year measurement period.
- Seasonal and diurnal patterns indicated significant low-level emissions.
- Seven main sources of H_2S were identified with a receptor orientated method.
- Source contributions above baseline concentrations were quantified.
- Urban areas were identified as an important source contributor of H_2S.

ARTICLE INFO

Keywords:
Hydrogen sulphide (H_2S)
Seasonal and diurnal patterns
Receptor source identification and quantification
South Africa
Air quality management

ABSTRACT

South Africa is one of the largest atmospheric sulphur emitting countries, but the contribution of H_2S to this regional burden is not known. Also, no H_2S source apportionment for South Africa have been undertaken, although H_2S has adverse effects on the environment and human health both directly and after being oxidised. Measurements were conducted for 2 years at a site on the Mpumalanga Highveld (South Africa), which is influenced by multiple sources. A mean of 3.1 ppb H_2S was obtained, which is similar than concentrations reported for some large Northern Hemisphere cities and areas close to gas processing plants. Well defined seasonal and diurnal patterns indicated that low-level emission sources likely made a significant contribution to the ambient H_2S concentrations. In this study, a receptor method was developed to enable identification of sources and quantification of their contribution to atmospheric H_2S levels above the baseline concentrations. The results indicate that emissions from urban areas on the Mpumalanga Highveld, associated with sources in towns, as well as semi- and informal settlements (e.g. ineffective household combustion of low grade coal, sewage waste water treatment facilities, landfills, small industries and traffic) contributed most to atmospheric H_2S levels in excess of baseline concentrations (34.6%), followed by pyrometallurgical smelters (19.8%) and a petrochemical operation near Secunda (17.9%). The Johannesburg-Pretoria megacity, coal-fired power stations, burning coal dumps and cattle feedlots contributed 10.9, 4.7, 3.8 and 0.4%, respectively, to H_2S concentrations in excess of the baseline levels, respectively. The results from this study will be informative for legislation that is currently being considered, wherein regional ambient H_2S standards for South Africa are suggested.

1. Introduction

Hydrogen sulphide (H_2S), together with sulphur dioxide (SO_2), carbonyl sulphide (OCS), carbonyl disulphide (CS_2) and dimethyl disulphide (CH_3SCH_3), are the principal sulphur containing compounds in the atmosphere (Seinfeld and Pandis, 2006). Rubright et al. (2017)

* Corresponding author. School of Physical and Chemical Sciences, North-West University, Potchefstroom, Private Bag x6001, Box 179, Potchefstroom, 2520, South Africa.
E-mail address: pieter.vanzyl@nwu.ac.za (P.G. van Zyl).

https://doi.org/10.1016/j.atmosenv.2023.120140
Received 14 June 2023; Received in revised form 28 September 2023; Accepted 10 October 2023
Available online 17 October 2023

summarised the pathophysiological responses associated with H_2S exposure, which starts with the odour threshold at approximately 10–15 ppb. Prolonged exposure at 2–5 ppm may cause nausea, tearing eyes, headache and loss of sleep. Exposure at 20 ppm could results in fatigue, loss of appetite, headache, irritability, poor memory and dizziness. Respiratory tract irritation may occur after 1-h exposure at 50–100 ppm. Depending on the concentration and exposure time, death may occur at exposure above levels of 100 ppm. In addition to the human pathophysiological effects, H_2S (−2 sulphur oxidation state) also contributes to impacts associated with SO_2 (+4 sulphur oxidation state), as well as sulphate and sulphuric acid (SO_4^{2-} and H_2SO_4; +6 sulphur oxidation state). This is due the atmospheric lifetime of H_2S typically only being 48 h (Seinfeld and Pandis, 2016), with it predominantly being oxidised to the afore-mentioned species. Sulphur +6 oxidation state compounds are commonly found in particulate matter (PM) that has atmospheric residence times of days to weeks depending on wet and dry deposition (Seinfeld and Pandis, 2016) and cause several adverse health effects (e.g. Di et al., 2017).

South Africa is regarded as the 9th largest atmospheric sulphur emitting country (Stern, 2006) and several studies have focused on the role of sulphur in wet deposition and process associated with atmospheric aerosols in the region. For instance, Conradie et al. (2016) reported SO_4^{2-} to be the dominant ionic species in wet deposition at sites located in industrial areas and the regional background in the north-eastern South African interior, while the average pH of wet deposition is low (i.e. pH 4.32 to 4.89) mainly due to the large fractional contribution of H_2SO_4. SO_4^{2-} (and/or H_2SO_4) also play an important role in new particle formation (NPF) and subsequent particle growth in the region (Vakkari et al., 2015). Sites in the South African interior have exhibited the highest annual median NPF frequencies and annual median growth rates measured internationally (Nieminen et al., 2018). In addition, SO_4^{2-} together with particulate organic matter (POM) have been reported to be the dominant species in submicron particles (PM_1) in the South African interior (Aurela et al., 2016; Tiitta et al., 2014; Venter et al., 2018).

Considering the above-mentioned, it is important to understand and quantify the possible contribution of H_2S to the atmospheric sulphur load in southern Africa. South African environmental legislation obliges large emitters of atmospheric pollutants to supply emission data to government. However, this occurs with some legal safeguards, which up to now has contributed to a comprehensive peer reviewed emission inventory not being available in the public domain. Therefore, atmospheric emission modelling studies for South Africa have to a large degree depended on global emission inventory databases (e.g. Kuik et al., 2015; Lourens et al., 2016), which do not always contain detailed information.

Within South Africa, the Mpumalanga Highveld is the region with the highest atmospheric sulphur load. The term Highveld refers to the inland plateau that has an altitude above ~1400 m above mean sea level (AMSL), which encompass almost the entire Free State and Gauteng Provinces, as well as significant portions of the surrounding Eastern Cape, Northern Cape, North West, Limpopo, and Mpumalanga Provinces (see Fig. 1 for details on provinces in South Africa). The Mpumalanga Highveld hosts an array of very large anthropogenic point and regional emission sources (Collett et al., 2010; Lourens et al., 2011). The atmosphere over this area is relatively heavily polluted (Department of Environmental Affairs, 2010) and an NO_2 hotspot over this region is clearly visible from satellite observations (e.g. Lourens et al., 2012).

As previously mentioned, the absence of atmospheric emission modelling studies for H_2S is at least partially due to the lack of a comprehensive peer-reviewed emission inventory. In addition, almost all receptor source apportionment studies conducted for South Africa have only been undertaken for atmospheric particulate matter (PM) (e.g. Engelbrecht et al., 2002; Jaars et al., 2018; Maenhaut et al., 1996; Tiitta et al., 2014; Van Zyl et al., 2014; Venter et al., 2017) and wet deposition (e.g. Conradie et al., 2016; Mphepya et al., 2004; Mphepya et al., 2006), without considering trace gases.

The general aim of this paper is to improve the understanding of ambient H_2S in southern Africa. The specific objectives were to contextualise the ambient H_2S concentration levels and explore temporal (seasonal and diurnal) patterns in order to gain insight into contributing sources/conditions above baseline H_2S concentrations. These aims will be achieved by considering a multi-year dataset collected at a representative site located in the Mpumalanga Highveld. This work will enable local and national government to identify and address emissions of H_2S, if required, in order to improve air quality and/or mitigate possible impacts thereof.

2. Method

2.1. Site description

Measurements were conducted from 1 February 2009 to 31 January 2011 during the South African measurement campaign, which was part of the European Integrated Project on Cloud Climate, Aerosols and Air Quality (EUCAARI) (Kulmala et al., 2011; Laakso et al., 2012) and conducted at the Elandsfontein measurement station (26° 14′43 S, 29° 25′30 E, 1750 m AMSL). As indicated in Fig. 1, this site was centrally situated with regard to most of the large point sources within the Mpumalanga Highveld, which limits bias to a specific source(s).

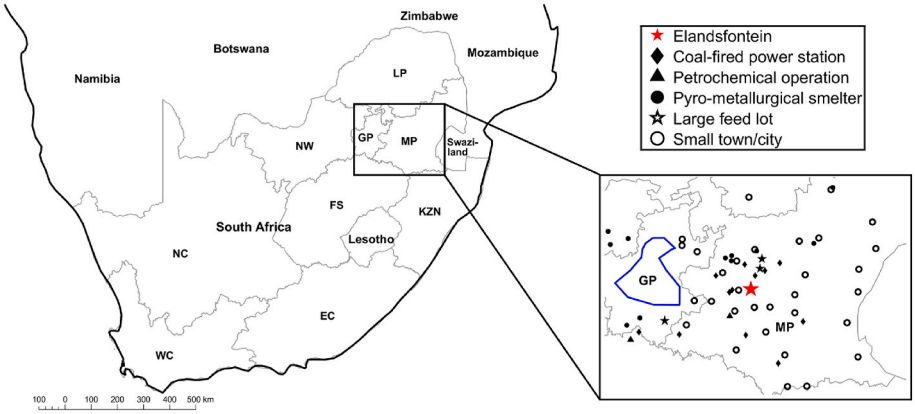

Fig. 1. Map indicating the position of the Elandsfontein measurement site in a southern African context. The blue polygon in the zoomed-in map indicates the Johannesburg-Pretoria megacity, while markers indicate the locations of various anthropogenic sources. The following abbreviations for the South African provinces were used: MP (Mpumalanga), GP (Gauteng), LP (Limpopo), NW (North West), FS (Free State), KZN (KwaZulu Natal), NC (Northern Cape), EC (Eastern Cape) and WC (Western Cape).

The immediate surroundings of the Elandsfontein site are mainly grazed grassland (Mucina and Rutherford, 2006), as clearly evident in the Google Earth image in Fig. S1, as well as cultivated land that is not evident from the Google Earth image. No large point sources occur within an approximate 15 km radius of the station. However, within a 100 km radius, numerous pyrometallurgical smelters, several coal-fired power stations and a large petrochemical operation are located (Collett et al., 2010; Laakso et al., 2012). In addition, there are also multiple other sources such as towns, landfills, burning coal dumps, large feedlots (>20 000 animals), traffic, open biomass burning, domestic fuel burning, waste burning, as well as marshlands and still standing water reservoirs. Another large source area is the Johannesburg-Pretoria (Jhb-Pta) megacity (depicted with a blue polygon in Fig. 1) with more than 10 million inhabitants, which is an area with many air quality issues (e.g. Lourens et al., 2012, 2016; Mathee and von Schirnding, 2003; Scorgie, 2012). From the afore-mentioned description it is evident that the region has a high density and diversity of atmospheric pollution sources, which makes it a complex area for a trace gas receptor orientated source identification and quantification study.

2.2. Measurements and instrumentation

H_2S, ozone (O_3), nitrogen oxides (NOx) and SO_2 were measured using a Thermo Electron 43A with a Thermo Electron 340 converter, a Monitor Europe ML9810B O_3 analyser, Thermo Electron 42i NOx analyser and a Thermo Electron 43C SO_2 analyser, respectively. Equivalent black carbon (eBC) (definitions according to Petzold et al., 2013) was measured with a Thermo Scientific model 5012 multi-angle absorption photometer (MAAP), for which eBC concentrations were corrected according to the algorithm presented by Hyvärinen et al. (2013). Meteorological measurements were taken with a Vaisala WXT510 meteorological station fitted on the roof of the measurement building at approximately 3.5 m above ground level and solar radiation with a PAR sensor (Laakso et al., 2012). All measurements were taken at 1-min. resolution, from which 15-min. averages were calculated, if at least two thirds of the data in the 15-min period was available. Data cleaning and quality assurance, as well as site maintenance procedures have previously been presented (e.g. Beukes et al., 2015; Laakso et al., 2012) and are therefore not repeated here.

Elandsfontein is an ESKOM operated ambient air quality measurement station (Collett et al., 2010), for which the instrument measurement set was significantly augmented during the EUCAARI project, e.g. scanning mobility particle sizer (SMPS) (Wiedensohler et al., 2012), optical particle counter (OPC), 3-wavelength particle soot absorption photometer (PSAP) (Backman et al., 2014), 3-wavelength Nephelometer (Venter et al., 2020), Cimel multichannel sunphotometer AERONET, 2020), dichotomous aerosol sampler with off line PM analyses (Venter et al., 2016) and a multi-wavelength Raman lidar (Giannakaki et al., 2015). However, these measurements were not considered in this paper and are therefore not discussed further.

2.3. Air mass history

The Lagrangian particle dispersion model FLEXPART (FLEXible PARTicle dispersion model) version 10.4 (Pisso et al., 2019; Seibert and Frank, 2004; Stohl et al., 2005) was used to calculate air mass histories to determine potential sources at the receptor site. According to Stohl et al., (1998), FLEXPART can be used backward in time to determine possible source contributions at receptor sites (Pisso et al., 2019). The European Centre for Medium-Range Weather Forecasts' (ECMWF) ERA5 reanalysis was used as inputs for FLEXPART. The resolution of the input data was 0.28125° over the 15°S −40°S and 10°E − 45°E area. The temporal resolution of the ERA5 was 1 h, while the vertical resolution was 137 model levels. Hourly arriving FLEXPART emission sensitivities were calculated for at least 48 h backwards, as this is estimated to be the approximate atmospheric lifetime of H_2S (Seinfeld and Pandis, 2006). FLEXPART emission sensitivities can be described as simulated particles that are modelled to be released backwards in time from a receptor site and their residence time within the output grid cells determines the sensitivity (Pisso et al., 2019).

2.4. Identification of burning coal dump locations

In order to identify the location and temporal activity of burning coal dumps in the area, the method presented by Beukes et al. (2018) was used. In the latter paper, fire radiative power (FRP) data obtained by the Moderate Resolution Imaging Spectro-radiometer (MODIS) instruments onboard the Terra and Aqua satellites was used to determine the availabilities of pyrometallurgical smelters (Beukes et al., 2018). This was conducted by identifying and tracking the activity patterns of false positive fires (sources that emitted radiative power signals, similar to open biomass burning), which were attributed to, for example, off-gas flaring and metal/slag tapping at pyrometallurgical smelters (Beukes et al., 2018). In the current study, the same method was used to determine the location and temporal activity of burning coal dumps within the study area, as presented in Cogho et al. (2022).

2.5. Identification and quantification of H_2S plumes

A novel receptor orientated technique to identify sources of atmospheric H_2S and quantify their relative contributions to above baseline concentrations of H_2S was developed in which a dataset comprising concurrently and continuously measured PM and trace gasses was used. This was done by modifying and improving a method presented by Chiloane et al. (2017). Although the aforementioned paper focussed on eBC, this method developed indicated the potential of being modified and applied to trace gases (Chiloane et al., 2017). In order to explain this technique, the algorithm developed is presented in Fig. 2. This algorithm has been programmed as a MATLAB script, but any similar programming language (e.g. R, Python) could be used.

The steps indicated in the algorithm (Fig. 2) are discussed in more detail below.

1) In the first step, the relevant data sets are loaded. In this case the Elandsfontein trace gases and eBC measurement data set, acquired during the EUCAARI project (Laakso et al., 2012), as well as hourly arriving FLEXPART back trajectories calculated for the entire measurement period, were loaded. Both datasets were in local time.
2) In the next step, 24hr ± 3hr time series concentration graphs for all the relevant species considered are plotted for visual inspection of gaseous plumes. 24hr ± 3hr time series graphs indicating increased concentrations of nitrogen oxide (NO), nitrogen dioxide (NO_2), SO_2, H_2S and eBC are presented in Fig. 3 as examples. The developed receptor orientated technique is based on the identification of co-incidental concentration peaks. Therefore, to ensure that a peak that extends over two consecutive days is correctly identified as a single peak, the ± 3hr periods are drawn with the specific 24hr period considered.
3) If visual inspection shows a peak in H_2S that can clearly be identified from the measurement noise and baseline concentration, we proceed to step 4. Otherwise, we move forward to the next day (i.e. step 2).
4) The user must now select the start and end times of the observed peak. If more than one such peak occurred, the most prominent one should be selected first. As is evident from the example presented in Fig. 3, there was a well-defined co-incidental peak from 09:07:30 to 13:35:30 (format HH:MM:SS), where H_2S peaked at the same time as NO, NO_2 and SO_2. Furthermore, to help the user classify/attribute the plume to the correct source or identify a source that was not initially included for selection, the user must

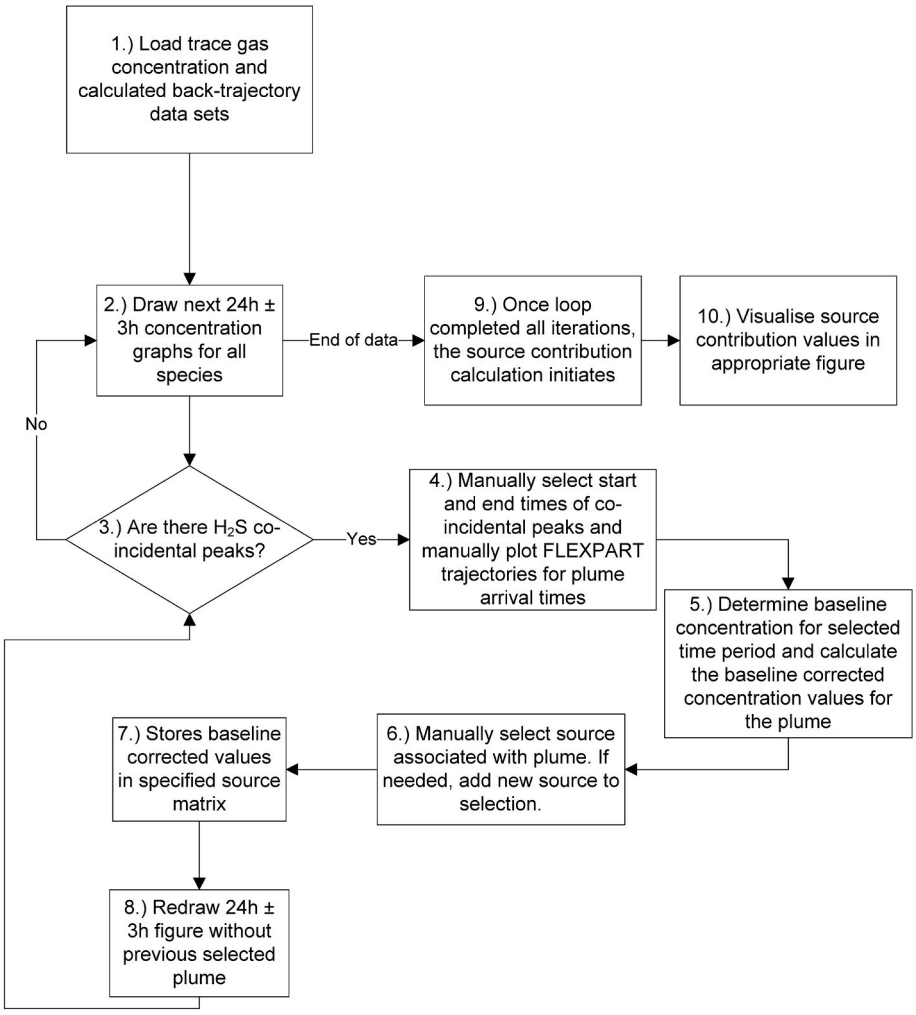

Fig. 2. Algorithm (flow diagram) for the novel source quantification method developed.

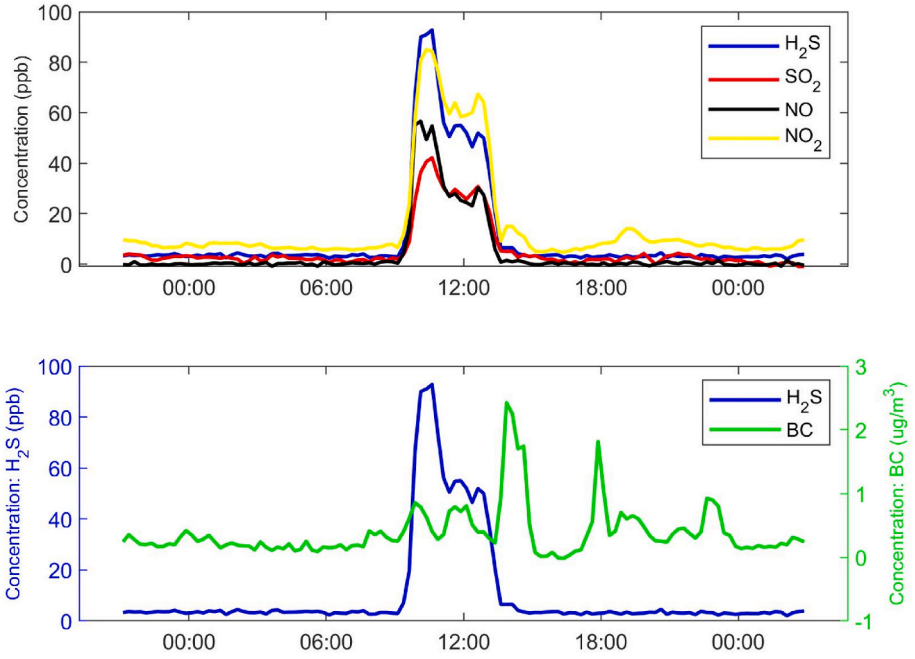

Fig. 3. Examples of 24hr ± 3hr time series concentration graphs for H_2S, SO_2, NO, NO_2 and eBC as retrieved on 1 June 2009.

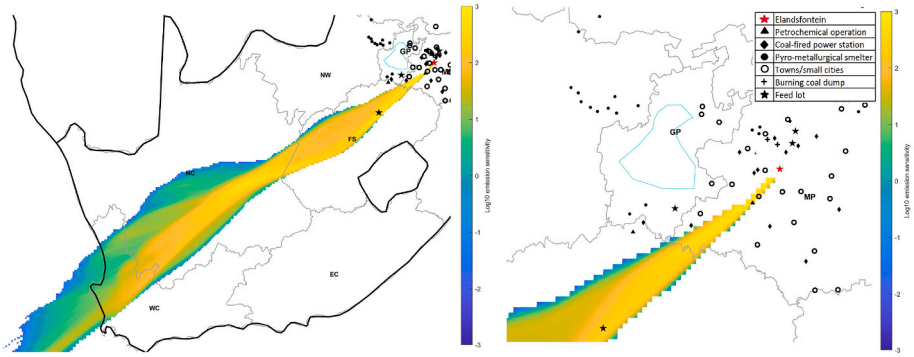

Fig. 4. Summarised FLEXPART air mass emission sensitivities for the example co-incidental H_2S plume depicted in Fig. 3. The markers indicate the location of sources, as defined in Fig. 1. On the left is the zoomed out FLEXPART emission sensitivities and the right side depicts a zoomed in version which helps to identify possible sources.

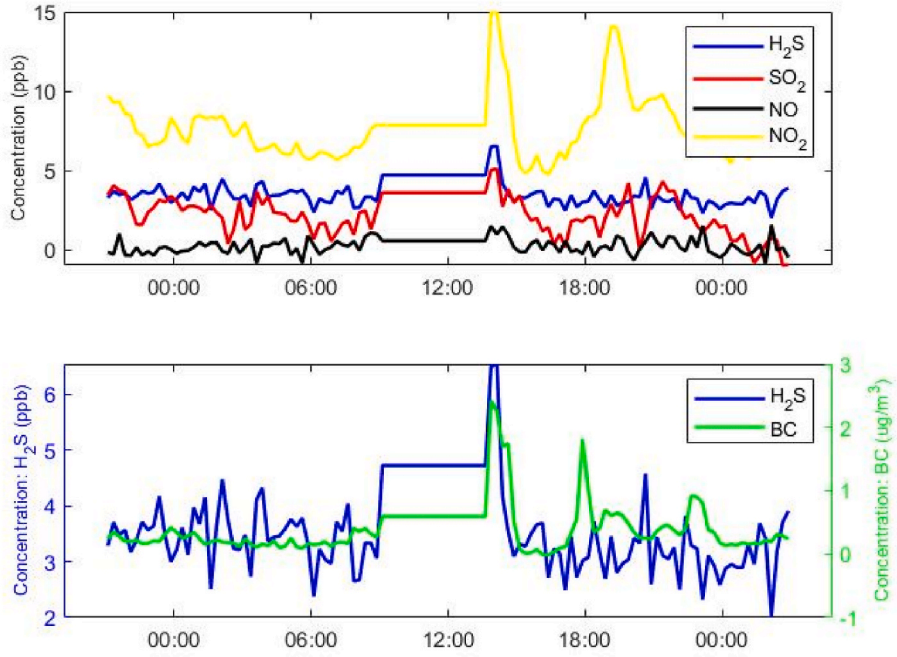

Fig. 5. Example 24hr ± 3hr time series concentration graphs for H2S, SO2, NO, NO2 and eBC on 1 June 2009, with the previously selected H2S and other co-incidental peaks (identified in Fig. 3) replaced by the baseline corrected value.

now manually plot the FLEXPART air mass emission sensitivities for each hour during the selected plume period (Fig. 4).

5) For the indicated plume period, the baseline H_2S concentration and baseline corrected plume concentrations are calculated. The baseline value is calculated as the average between the start and end H_2S concentrations of the plume, while the H_2S plume baseline corrected concentrations are calculated by subtracting the baseline value from each 15-min average concentration during the selected plume period.
6) Now, potential sources of the identified H_2S plume are considered. Sources were grouped into the following categories: petrochemical operation near Secunda, coal-fired power stations, pyrometallurgical smelters, the Jhb-Pta megacity, feedlots, the paper mill near Nelspruit, emissions associated with towns/small cities/in- and semiformal settlements (which include waste water treatment facilities, landfills, household combustion emissions, small industries, as well as vehicle emissions, especially from older diesel engines) and mixed/undefined sources. This categorization is performed by considering all the relevant information available for each plume. For instance, co-incidental increases in certain species can be expected from certain sources and different sources might have different plume amplitude strengths. For the specific plume example presented in Figs. 3 and 4, four complementary pieces of evidence indicated that the measured H_2S plume originated from the petrochemical operation near Secunda with very high probability. Firstly, the plume amplitude was relatively large, which is not expected for regional sources. Secondly, the increase in H_2S concentration coincide with increased NO, NO_2 and SO_2 levels, but not with eBC (Fig. 3), which is typically associated with open biomass burning. The petrochemical operation generates a significant fraction of its own electricity, therefore NO, NO_2 and SO_2 emissions will coincide with H_2S. Additionally, Chiloane et al. (2017) showed that the specific petrochemical operation considered here did not significantly contribute to eBC measured at Elandsfontein, therefore the absence thereof in this plume is expected. Thirdly, the timing of the identified plume corresponds to a typical high-stack emission that mixes down to surface after the breakup of the low-level inversion layer(s), which typically occurs between 08:00 and 10:00 local time as the depth of the planetary

boundary layer (PBL) starts to increase at Elandsfontein (Korhonen et al., 2014), as well as on the Highveld in general (Gierens et al., 2018). Lastly (4th), the source assumption was also supported by considering the corresponding air mass history information (Fig. 4), since the calculated FLEXPART emission sensitivity during the plume period passed very close to the petrochemical operation. In addition to the petrochemical associated plume example considered here (Figs. 3 and 4), more examples in the form of case studies are presented in Section 3.4 and criteria for the different source categories are summarised in Table 1 below.

7) Once the source category is identified, the plume baseline corrected concentration values of H_2S are stored in the data matrix for that particular source. For the example plume considered here in Figs. 3 and 19 plume baseline corrected 15-min average H_2S concentration values (09:07:30 ≤ period ≤13:35:30) were stored in the source matrix of the petrochemical operations.
8) In this step the program redraws the considered 24h ± 3h time series concentration graphs for further visual inspection, as indicated in Fig. 5, and the process continues by going back to step 4 (Fig. 2). However, in these graphs the previously attributed plume concentrations are replaced with the baseline corrected value calculated in step 7 and the y-axes of the graphs (species concentrations) are automatically rescaled to enable easier identification of possible smaller (lower concentration) co-incidental peaks.
10) Once the analysis of the full data set is completed, the source contribution calculation initiates (step 11). In this calculation, <u>Equation (1) is applied to each of the source matrices. This equation calculates the percentage contributions to H_2S measured above the baseline concentrations for each of the identified sources.

$$\%\ Source\ contribution = \frac{Cs}{Tc} \text{ x } 100 \quad (1)$$

Where C_s is the sum of all the plume baseline concentration corrected values that were attributed to the specific source; and T_c is the sum of all the plume baseline corrected concentrations that were attributed to all the source matrices. Additionally, the baseline H_2S concentration for the entire measurement period is also calculated from the average concentrations remaining after all attributed plume concentrations have been replaced by the plume-specific baseline values.

11) Finally, an appropriate figure (and table with actual values) is compiled to visualise the H_2S source quantifications in terms of H_2S above the baseline concentrations, as well as provide ratios of baseline corrected H_2S concentrations divided by baseline corrected concentrations of the other species relevant to each

Table 1
Criteria for selection of possible sources based on type of pollutants, meteorological conditions, plume characteristics and plume timings.

Source	fx1H_2S	NOx	SO_2	BC	Plume characteristics	Timing	FLEXPART
Petrochemical	Present	Present, ratios of NO and NO_2 differ depending on plume age	Present	Absent	Strong well defined plumes, very high concentrations	Typically, during daytime after the break-up of inversions and PBL's	Finally for all occasions FLEXPART emission sensitivity analysis is used as a last filter to determine if the source identification was correct
Power stations	Rarely present and concentration much lower than other co-incidental species	Present, ratios of NO and NO_2 differ depending on plume age	Present	Present	Strong well defined plumes, very high concentrations except for H_2S	Typically, during daytime after the break-up of inversions and PBL's	
Pyrometallurgical smelters	Present	Present, ratios of NO and NO_2 differ depending on plume age	Present and typically higher than other co-incidental species	Present and typically higher than in other combustion sources	Strong well defined plumes	Are seen throughout the day as stacks emit below PBL's	
Urban	Present	Present, ratios of NO and NO_2 differ depending on plume age	Present	Present	Plume amplitude typically not large, but the duration of plumes are usually long	Typically, during night time and early mornings as PBL depth is shallow and low level emissions are common	
Jhb/Pta	Present	Present, ratios of NO and NO_2 differ depending on plume age	Present	Present	Plume amplitude typically not large, but the duration of plumes are usually long	Typically, during night time and early mornings as PBL depth is shallow and low level emissions are common	
Burning coal dumps	Present	Present, ratios of NO and NO_2 differ depending on plume age	Present	Present	Weak plume amplitudes and strength compared to other sources	Typically, during night time and early mornings as PBL depth is shallow and low level emissions are common	
Feedlots	Present	Present, ratios of NO and NO_2 differ depending on plume age	Sometimes, probably due to fractional oxidation of H_2S to SO_2	Absent as there are rarely any combustion activities at the feedlots	Weak plume amplitudes and strength compared to other sources	Typically, during night time and early mornings as PBL depth is shallow and low level emissions are common	

source type. Since so little H_2S data is available for South Africa, such ratios can be used in future modelling studies as approximated emission factors to estimate H_2S if only concentration(s) of other species are known.

3. Results and discussion

3.1. Data coverage and contextualisation

H_2S data coverage during the measurement period was approximately 75%. Most of the data gaps were due to electrical power outages, since South Africa was overwhelmed by an energy crisis at the time (Pretorius et al., 2015). Additionally, questionable and/or uncertain data points were removed to ensure a high-quality data set, as per the previously published quality control procedures (Beukes et al., 2015; Laakso et al., 2012). Considering that most of the data gaps were due to power outages and that the dataset was subjected to thoroughly quality procedures, the 75% data coverage can be considered relatively good. Additionally, gaps in data occurred throughout the entire measurement period and were not associated with specific periods, which therefore avoid seasonal bias.

In Table 2, the mean and median, as well as 5th, 25th, 75th and 95th percentile H_2S concentration values for the entire study period are presented. The mean H_2S concentration of 3.1 ppb was significantly higher than mean concentrations reported for real background sites such as over the northern equatorial Atlantic Ocean and rural regions of France where mean H_2S concentrations of 5–50 ppt (0.005–0.05 ppb) and 0.055 ppb were respectively recorded (Slatt et al., 1967; Delmas et al., 1980). The mean of 3.1 ppb was similar than the mean concentration of 5.55 ppb reported for the city of Thessaloniki, Greece (Kourtidis et al., 2007), as well as to a residential area in Arkansas, USA in proximity of gas processing plants where mean concentrations of 2.4 and 3.4 ppb were recorded for May to July and October to December 1998, respectively (Skrtic, 2006). However, the mean H_2S concentration at Elandsfontein was significantly lower than the mean levels reported for heavily H_2S polluted sites such as Whakarewarewa Village in the city of Rotorua in New Zealand for which a mean ranging between 66 and 100 ppb was recorded (Bates et al., 2013; Hinz, 2011), which was attributed to the proximity of an active geothermal field.

Currently there is no South African National Ambient Air Quality Standard (NAAQS) limit value for ambient H_2S. However, the South African Department of Environmental Affairs (DEA) stipulates that if a one-hourly average H_2S concentration exceeds 29 ppb on any specific day, this day is regarded as a high H_2S day (DEA, 2010). The calculated hourly average H_2S levels exceeded this 29 ppb "standard limit" 47 times on 13 days. In Table 3, the timestamp, concentration and source associated with each of these exceedances are presented. Therefore, 13 "high H_2S days" were recorded at Elandsfontein during the two-year measurement period. Considering the average SO_2 concentration of 11.5 ppb determined at Elandsfontein (Laakso et al., 2012), it appears that >20% of gas phase sulphur is in the form of H_2S.

Table 2
Mean and median, as well as the 5th, 25th, 75th and 95th percentile concentration values for H_2S over the entire measurement period.

Description	Value (ppb)
Mean	3.1
Median	1.8
5th Percentile	0.4
25th Percentile	1.1
75th Percentile	3.2
95th Percentile	11.1

3.2. Temporal H_2S patterns

Statistical distribution of monthly H_2S concentrations measured at Elandsfontein are presented in Fig. 6. For referencing purposes, the 5th, 25th, 75th and 95th percentile concentration values are presented in Table S2. It is evident from Fig. 6 that H_2S concentrations were generally higher in the colder (May to August) and/or dryer (May to mid-October) months, and lower in the wetter (mid-October to April) and/or warmer (September to April) months (seasonal classification according to Venter et al., 2020). This indicates that low-level emission sources likely make a significant contribution to ambient H_2S measured at Elandsfontein, since these emissions are trapped and concentrated by low-level thermal inversion layers and/or a shallow PBL depth. Such conditions are particularly common over the South African Highveld during night-time and early mornings during the colder months (Garstang et al., 1996; Gierens et al., 2018; Korhonen et al., 2014), which reduce vertical mixing in the troposphere.

In Fig. 7, the overall diurnal pattern (for the entire measurement period), as well as diurnal patterns for the different seasons (Summer = DJF; Autumn = MAM; Winter = JJA; Spring = SON) are depicted. It is evident that H_2S concentrations were highest in winter (red line), which agrees with the seasonal analysis considered in Fig. 6. In general, the diurnal patterns are characterised by bimodal peaks, occurring in the early morning (between approximately 04:00 and 08:00) and evening (after approximately 19:00), which also corresponds to low-level emissions being trapped by a low-level inversion layer(s) and/or a shallow PBL depth (Garstang et al., 1996; Gierens et al., 2018; Korhonen et al., 2014). Additionally, lower O_3 and hydroxyl radical ($OH^{\bullet}$) concentrations during night-time (Laban et al., 2018; Gierens et al., 2004), with associated less oxidation of H_2S, could contribute to the higher H_2S levels during night-time. A H_2S peak is also observed between 9:00 and 13:00 in all the diurnal patterns, which is indicative of downward mixing of high stack emissions after the break-up of the aforementioned inversion layer(s) and growth of the PBL (Garstang et al., 1996; Gierens et al., 2018; Korhonen et al., 2014). This peak is particularly prominent in winter due to more frequent and pronounced thermal inversion layers, as well as a lower PBL depth over the South African Highveld during this time of the year (Garstang et al., 1996; Gierens et al., 2018; Korhonen et al., 2014).

3.3. Example case studies of prominent sources

In this section, example case studies will be presented to further illustrate how plumes from major sources were identified and related to the sources. Since an example for the petrochemical operations was already presented in Section 2.5, an example for this source type is not repeated here. In addition, a table that describes the chemical characteristics/footprint of each source was presented in Table 1 to further explain how the sources were differentiated.

3.3.1. Urban plumes

As previously stated, the term "urban" within the context of this study refers to plumes associated with a town/city/in- or semiformal settlement, which excluded the Jhb-Pta megacity. Fig. 8 presents a Google Earth image of the small-town Bethal, which is approximately 25 km from Elandsfontein. It is evident that this town has a number of regions that holds different sources from which H_2S can be emitted, e.g. residential coal burning for heating and cooking purposes in informal settlements, industrial activities and waste treatment facilities in the small industrial area, as well as vehicle emission from all the areas in this town. Due to the relatively small size of each individual source and the close proximity thereof to one another, such sources were considered as a single source area of H_2S, i.e. "urban", in the source quantification.

In Fig. 9 increases in H_2S, SO_2 and NO_2 are observed, together with a small increase in eBC, but no increase in NO, between 14:00 and 17:00 on the 10th of January 2011. As previously indicated, a peak with

Table 3
Hourly exceedances of 29 ppb H_2S high day threshold value and the respective sources.

Date and Time	Source	Concentration (ppb)	Date and Time	Source	Concentration (ppb)
2009/04/18 03:00	Urban	34.98	2009/09/18 11:00	Jhb/Pta	48.61
2009/04/24 06:00	Pyrometallurgical smelter	36.75	2009/12/18 05:00	Jhb/Pta	46.83
2009/04/24 07:00	Pyrometallurgical smelter	30.92	2009/12/23 02:00	Coal Dump	36.3
2009/04/24 08:00	Pyrometallurgical smelter	33.35	2009/12/23 03:00	Coal Dump	30.35
2009/04/25 02:00	Pyrometallurgical smelter	31.83	2010/05/24 03:00	Urban	33.46
2009/05/16 05:00	Coal-fired Powerstation	31.38	2010/05/24 15:00	Petrochemical	32.05
2009/05/19 14:00	Coal-fired Powerstation	34.91	2010/05/24 16:00	Petrochemical	42.31
2009/05/19 15:00	Coal-fired Powerstation	33.98	2010/05/24 17:00	Petrochemical	38.67
2009/06/01 10:00	Petrochemical	66.75	2010/06/05 15:00	Petrochemical	52.33
2009/06/01 11:00	Petrochemical	68.23	2010/06/05 16:00	Petrochemical	60.83
2009/06/01 12:00	Petrochemical	52.11	2010/06/05 17:00	Petrochemical	44.76
2009/06/01 13:00	Petrochemical	39.82	2010/06/05 18:00	Petrochemical	32.22
2009/06/03 01:00	Jhb/Pta	34.47	2010/06/06 16:00	Urban	33.5
2009/06/28 10:00	Petrochemical	37.42	2010/06/06 17:00	Urban	33.65
2009/06/28 11:00	Petrochemical	74.61	2010/06/08 06:00	Urban	71.68
2009/06/28 14:00	Petrochemical	41.03	2010/06/21 21:00	Combination	30.87
2009/06/28 15:00	Petrochemical	32.25	2010/06/21 22:00	Combination	31.36
2009/07/02 02:00	Coal Dump	29.88	2010/06/23 01:00	Jhb/Pta	36.45
2009/07/03 03:00	Coal Dump	38.74	2010/06/23 04:00	Jhb/Pta	33.52
2009/07/09 13:00	Petrochemical	29.57	2010/07/16 10:00	Petrochemical	30.01
2009/07/10 20:00	Urban	37.49	2010/08/14 12:00	Petrochemical	32.85
2009/07/12 00:00	Urban	42.01	2010/09/27 10:00	Urban	31.42
2009/08/20 10:00	Petrochemical	42.11	2010/11/20 11:00	Jhb/Pta	53.57
2009/09/15 23:00	Urban	32.43			

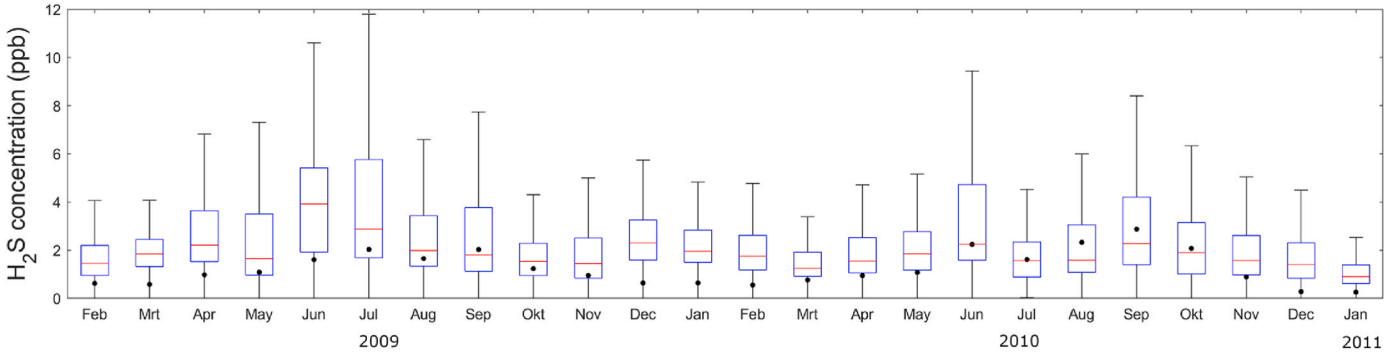

Fig. 6. Box-and-whisker plots of the measured H_2S concentrations for each month during the study period. The red line represents the median, the black dot the mean, the box the 25th and 75th percentiles and the whiskers are equal to 1.5 times the interquartile range.

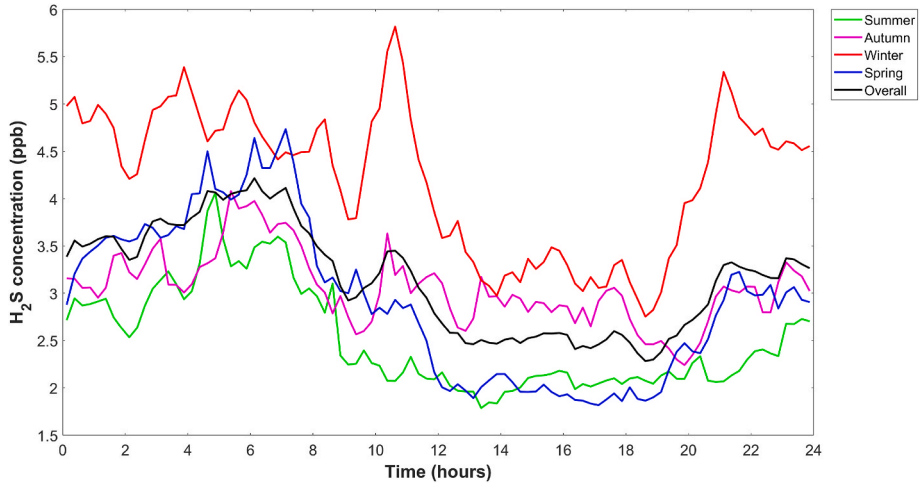

Fig. 7. Diurnal patterns based on average 15-min data of H_2S for the entire measurement period, as well as for each season (Summer = December, January and February; Autumn = March, April and May; Winter = June, July and August; Spring = September, October and November).

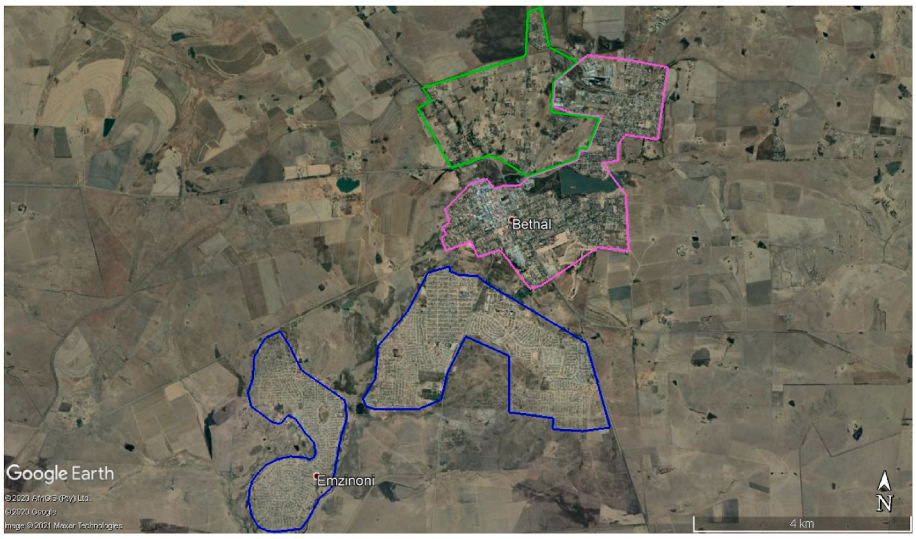

Fig. 8. Google Earth image of the small town of Bethal. The purple polygon indicates the formal residential, small industry and business areas of Bethal, while the blue polygons the semi- and informal settlements. The surrounding area consist of small agricultural holdings (green polygon), as well as larger farmlands.

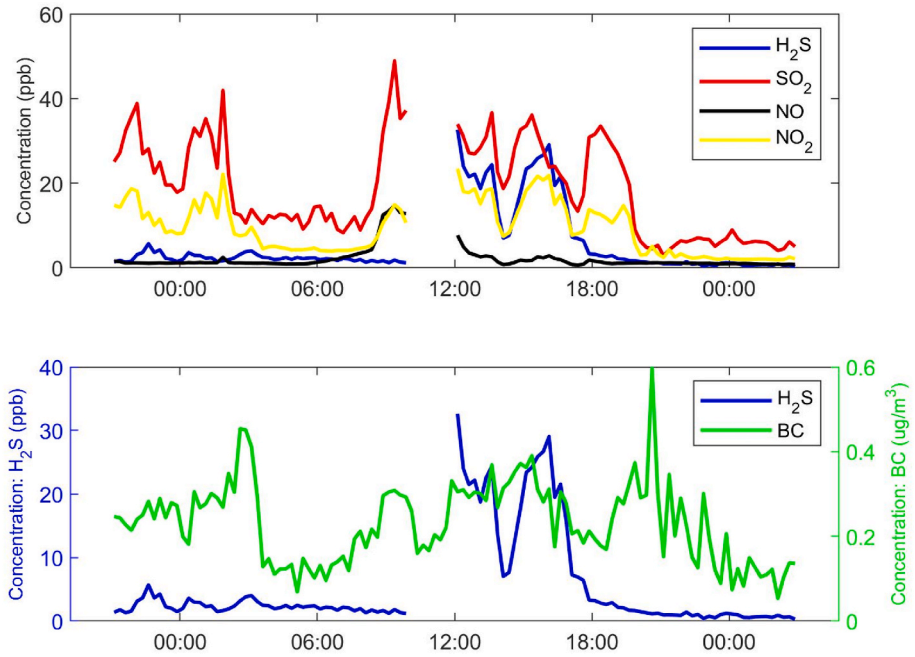

Fig. 9. 24hr ± 3hr time series concentration graphs of co-incidental increases of H_2S, SO_2, NO_2 and eBC on the 10th of January 2011.

coincidental increase of these species is indicative of household combustions on the Mpumalanga Highveld (Chiloane et al., 2017). Although roughly 90% of households in South Africa are electrified, it is estimated that more than 70% of low-income households are mainly dependent on fuels such as coal, firewood and kerosene (Mbonane et al., 2018). Coal is the most abundant fuel source for residential burning in the Mpumalanga province due to its availability and low cost (Balmer, 2007; Langerman et al., 2018; Mbonane et al., 2018). Ineffective household combustion processes applied, especially in in- and semiformal settlements do not oxidise all the sulphur in the fuel to SO_2, therefore H_2S can also be emitted. It was found that low ventilation coal stove emissions can contain more than 800 ppm H_2S during pyrolysis and about 900 ppm SO_2 during the coking phase (Makonese et al., 2015).

The timing of the co-incidental concentration peaks (Fig. 9) does not exclude the possibility of high stack emissions (e.g. from coal-fired power stations, or a petrochemical operation) as the plume is observed during daytime when strong inversions are not present and the PBL is higher (compared to early mornings and night-time), which will allow downward mixing of high stack pollutants (Garstang et al., 1996; Gierens et al., 2018; Korhonen et al., 2014). However, air mass history indicates strong emission sensitivity over the nearby town Bethal (Fig. 10), as well as other small towns within the area. Although air mass history in Fig. 10 indicates the possible influence industry, i.e. a small fraction of air masses passing over industrial point sources, lower emission sensitivities were associated with these sources in this case study. Considering the aforementioned, this plume was attributed to the "urban" source type.

3.3.2. *The Jhb-Pta megacity*

The Jhb-Pta megacity was categorised separately from the other urban sources in this study since it is a very large conurbation compared to other urban areas. In Fig. 11, co-incidental increases in levels of H_2S,

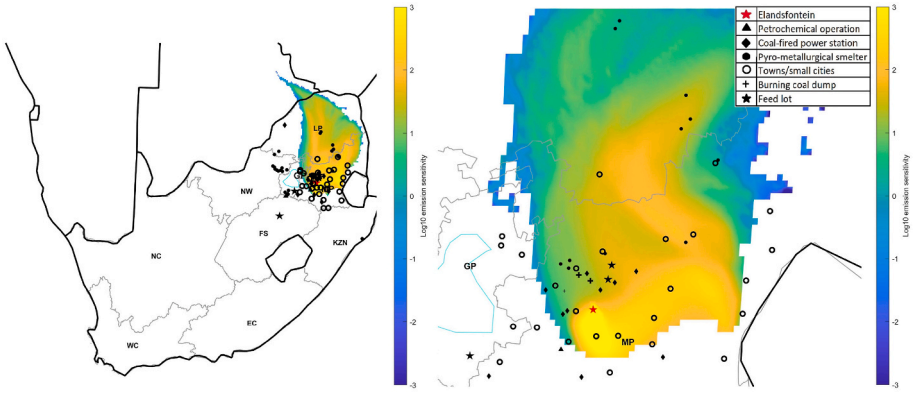

Fig. 10. Summed up FLEXPART emission sensitivities for the example co-incidental H_2S plume depicted in Fig. 9.

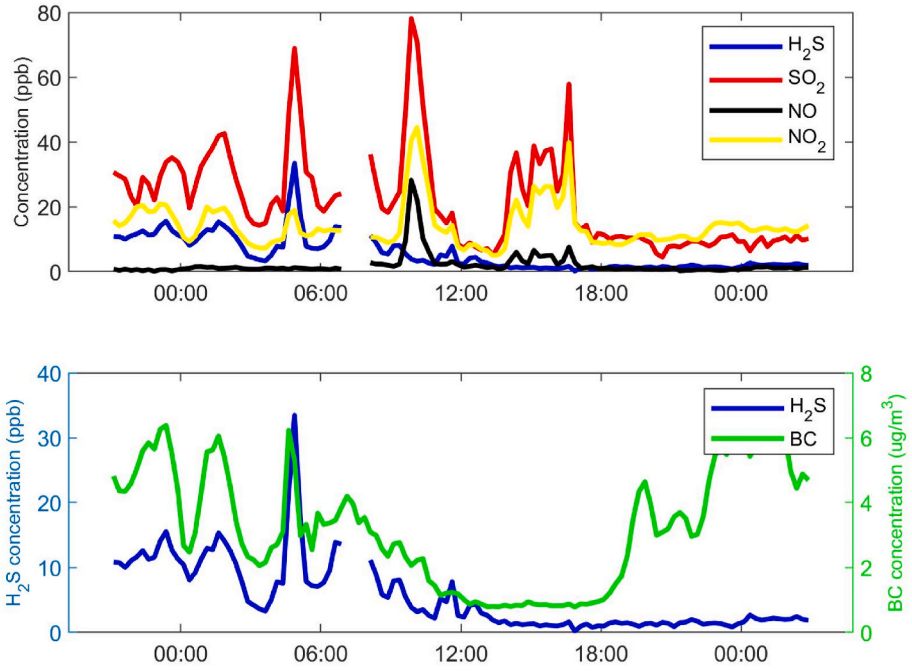

Fig. 11. 24hr ± 3hr time series concentration graphs of co-incidental increases of H_2S, SO_2, NO_2 and eBC between 00:00 and 03:00 on the 26th of August 2009.

SO_2, NO_2 and eBC are evident between 00:00 and 03:00 on the 26th of August 2009, but no NO was observed. The Jhb-Pta megacity is further from the measurement site than the smaller towns/cities/settlements in this region, which allows more time for O_3 to react with NO to produce NO_2 during night-time transport.

The timing of the co-incidental concentration peaks suggests low-level emissions to be the origin as it is observed early morning, which makes it very unlikely that downward mixing of high stack pollutants

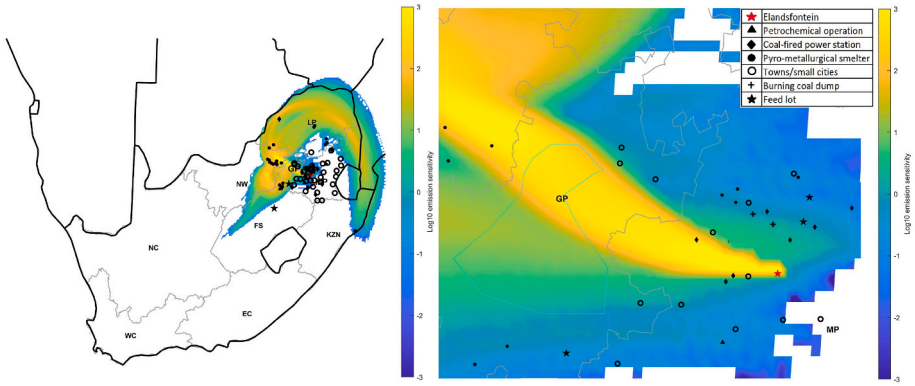

Fig. 12. Summed up FLEXPART emission sensitivities for the example co-incidental H_2S plume depicted in Fig. 11.

would occur (Garstang et al., 1996; Gierens et al., 2018; Korhonen et al., 2014). Air mass history in Fig. 12 also indicated air masses passing over the Jhb-Pta megacity (blue polygon) and close to a coal-fired power plant, but the absence of NO rules out influence of fresh power plant emissions. Although further upwind air mass passed over pyrometallurgical smelters in the wester BIC, their influence is considered small in relation to the number of air masses passing over the Jhb-Pta conurbation (Fig. 12). Considering all the aforementioned, it is likely that the plume is dominated by the Jhb-Pta megacity emissions.

3.3.3. Pyrometallurgical smelters

Plumes from pyrometallurgical smelters on the Mpumalanga Highveld are usually characterised by coincidental increases of SO_2, NO_2 and eBC, together with H_2S (Chiloane et al., 2017). H_2S in these plumes are expected, since pyrometallurgical smelting is a reductive process that is conducive to the formation of H_2S. However, a significant fraction of the H_2S will be oxidised to SO_2 during off-gas combustion above the material bed in open and/or semi-closed furnaces (Beukes et al., 2017), or during flaring of cleaned off-gas by closed furnaces (Du Preez et al., 2015; Beukes et al., 2017). In Fig. 13, the co-incidental increase of H_2S, SO_2, eBC and some NO_2 is observed between 04:00 and 10:00 on the 24th of April 2009, which is the first indication that this plume might have originated from a pyrometallurgical smelters.

One would expect emissions from pyrometallurgical smelters to be released *via* high stacks. However, in South Africa the stacks of pyrometallurgical smelters are typically not very tall. For example, the highest stack at the Lion Ferrochrome smelter of Glencore in Steelpoort is 58 m and on average the stacks at this smelter are just 45 m tall (Air Resources Laboratory, 2014). According to the Rustenburg Local Municipality air quality management plan (Piketh et al., 2005), only some platinum group metal (PGM) smelters have stacks that are higher than 100 m, while most other smelters typically have stacks lower than 50 m. PGM smelters emit significant quantities of SO_2 since they consume sulphide-rich ore (Xiao and Laplante, 2004). However, on the Mpumalanga Highveld there are no PGM smelters, just ferrochrome, ferromanganese and ferrovanadium smelters, as well as a steel mill. Therefore, these pyrometallurgical smelters will emit pollutants below low-level thermal inversion layer(s) (Gierens et al., 2018) over the Highveld, where it can be trapped and concentrated during night-time and early mornings. Plumes from these smelters could therefore be observed at Elandsfontein during any time of the day. It is evident from Fig. 14 that air masses arriving at 06:00 at Elandsfontein on this specific day passed over three pyrometallurgical smelters that are located in the Witbank area, which are most likely the main source of H_2S in this case study.

3.3.4. Coal-fired power stations

It was not expected to observe significant H_2S emissions associated with coal-fired power station at Elandsfontein, since boilers at these facilities burn at exceptionally high temperatures (~1200 °C at full load, ESKOM, 2019) in an oxidising environment. However, H_2S was observed in some plumes from coal-fired power station and therefore two case studies are presented. The first will be, what is considered, a normal (more common) coal-fired power station plume without H_2S, while the second case study will investigate, a less commonly observed coal-fired power station plume with H_2S being present.

3.3.4.1. Coal-fired power station plume without H_2S. Typically, plumes associated with high stack coal-fired power generation emissions in the South African interior are observed at ground level after growth of the PBL depth and breakup of low-level thermal inversion layer(s) in the morning. This often results in a sharp increase in pollutant concentrations as downward mixing occurs. Such a plume is visible in Fig. 15, where a sharp increase in SO_2, NO_2 and NO, but not H_2S, was observed between 11:00 and 17:00 on the 11th of May 2009, suggesting that these species are emitted from a coal-fired power station (Collett et al., 2010; Lourens et al., 2011). Furthermore, air mass history (with a starting time at 10:00) also reveal that air masses passed over two coal-fired power stations in Fig. 16. Taking into account the co-incidental increases of NO, NO_2 and SO_2, the timing and amplitude of the co-incidental increases, and air mass origin, it is evident that the plume originated from the coal-fired power stations.

3.3.4.2. Coal-fired power station plume with H_2S. As indicated in Fig. 17, coincidental increases in SO_2, NO_2, eBC and H_2S were observed between 17:00 and 19:00 on the 26th of May 2010. The absence of NO in the plume is indicative of an aged plume with NO being oxidised to NO_2. As

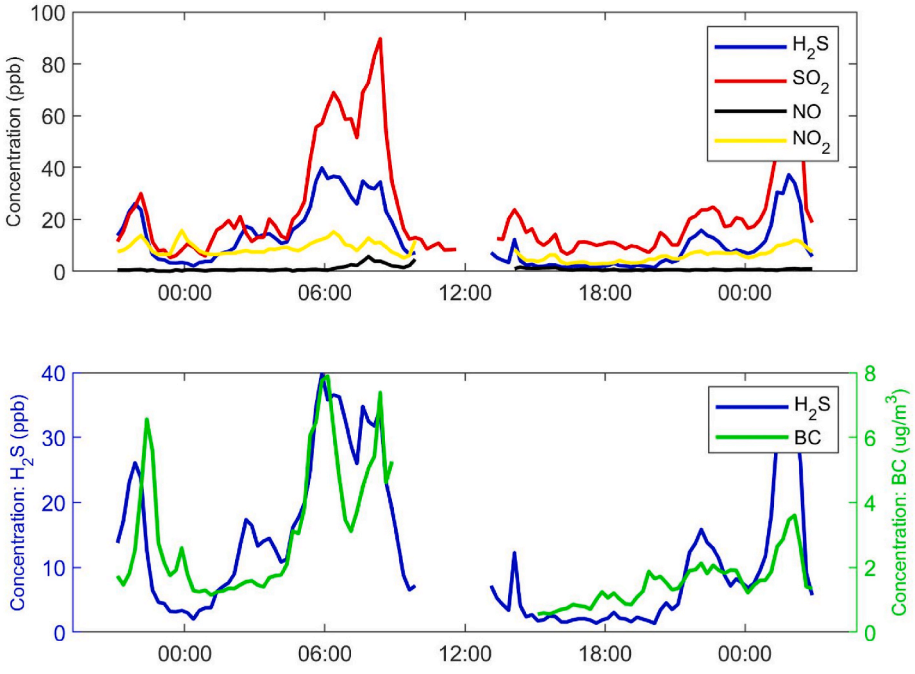

Fig. 13. 24hr ± 3hr time series concentration graphs of co-incidental increases of H_2S, SO_2, NO, NO_2 and eBC on the 24th of April 2009.

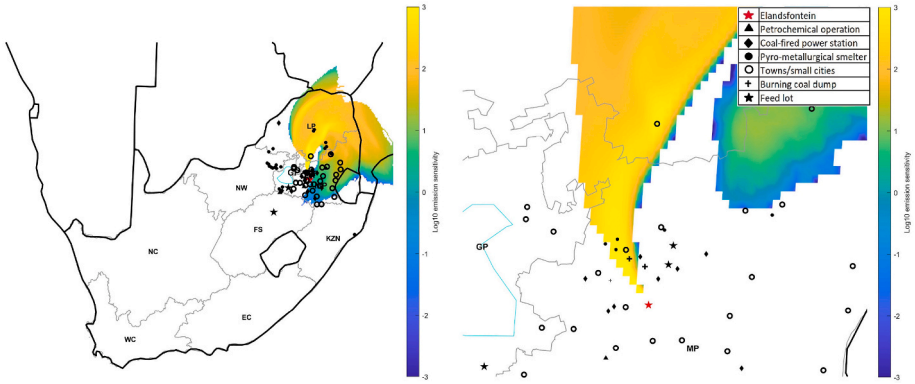

Fig. 14. Air mass history for the example co-incidental H_2S plume depicted in Fig. 13.

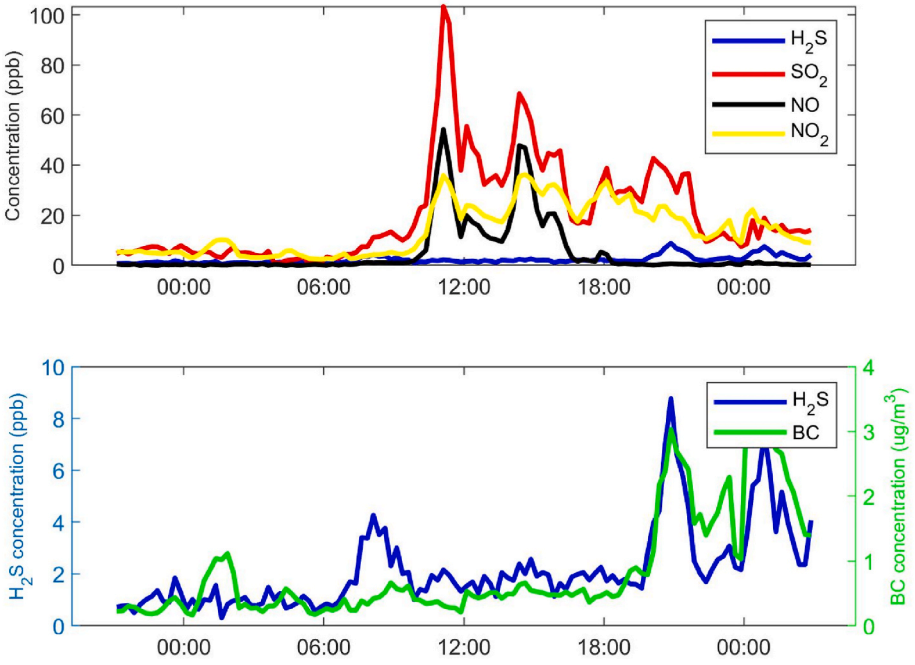

Fig. 15. 24hr ± 3hr time series concentration graphs of co-incidental increases of SO_2, NO and NO_2 between 11:00 and 17:00 on the 11th of May 2009.

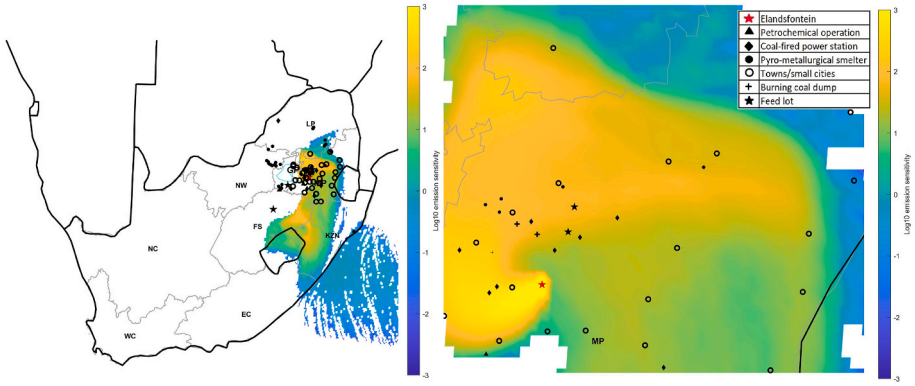

Fig. 16. Summed up FLEXPART emission sensitivities for the example co-incidental H_2S plume depicted in Fig. 15

explained earlier, the timing and amplitude of the co-incidental peak suggest that the plume is of high stack origin, i.e. either from a coal-fired power station or the petrochemical operation near Secunda. Due to the presence of H_2S in the co-incidental peaks considered in this case study, it could very easily be assumed that the plume originated from the petrochemical operation. However, the emission profile does not look similar than that of a petrochemical operation. H_2S is evident as a peak, that has approximately the same profile as the observed NO_2 and SO_2,

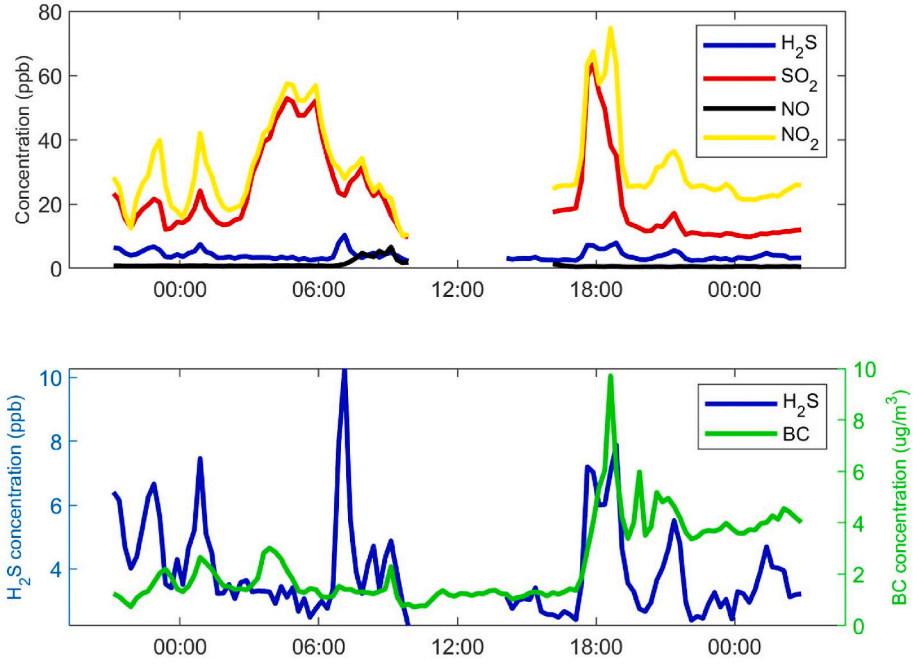

Fig. 17. 24hr ± 3hr time series concentration graphs of co-incidental increases of H_2S, SO_2, NO and NO_2 on the 26th of May 2010.

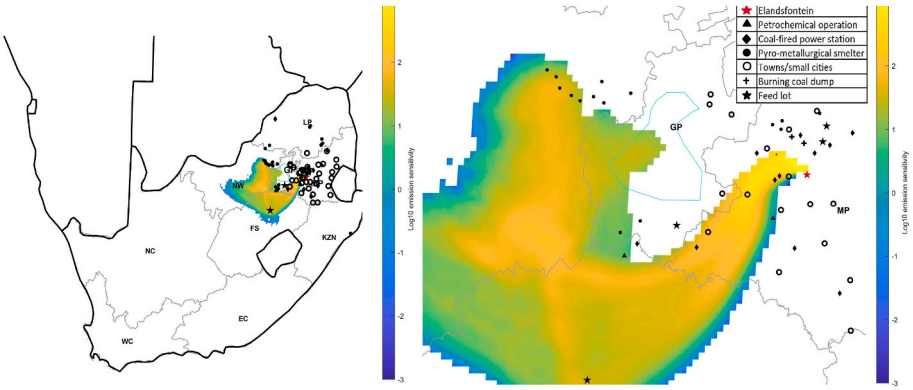

Fig. 18. Summed up FLEXPART emission sensitivities for the example co-incidental H_2S plume depicted in Fig. 18.

but it is not as concentrated. In addition, the co-incidental increase in eBC is not present in plumes associated with the petrochemical operation. It is also evident from air mass history for this case study (Fig. 18) that air masses passed over or close to coal-fired power plants to the west of the Elandsfontein station.

As indicated earlier, it is well known that pollution from coal-fired power stations in South Africa are characterised by coincidental increases in SO_2, NO_2 and NO (Collett et al., 2010; Lourens et al., 2011; Belaid et al., 2014; Pretorius et al., 2015). However, according to Shirai et al. (2012), it is possible for H_2S to be formed during coal-fired power generation if low-NO_x combustion principles are applied. Several papers have been published that indicate that the sole electricity supplier in South Africa, ESKOM, have indeed been switching to low-NO_x burners in order to move closer to compliance with more stringent NO_x emission standards (e.g. Engineering News, 2017; Van der Merwe et al., 2017). Another reason for the presence of H_2S is that a non-ideal oxidative environment is experienced when a coal-fired boiler is started up, which could lead to some H_2S also being emitted. Typically, a cold boiler is initially started by injecting fuel oil at a high pressure through nozzles (ESKOM, 2019), which does not represent boiler conditions at full load and temperature (ESKOM, 2019). South Africa has been in an energy crisis since 2007 due to an increase in electricity demand and poor maintenance of the coal-fired power stations (Pretorius et al., 2015). These factors have resulted in more than normal breakdowns (and associated cold start-ups) of coal-fired power station boilers.

3.3.5. *Cattle feedlots*

There are three large cattle feedlots relatively close to the Elandsfontein measurement station with Fig. 19 depicting a Google Earth image of the Kanhym feedlot (25° 53′40 S, 29° 33′31 E). These feedlots emit pollutants at surface level and are characterised by emissions of reduced sulphur compounds such as H_2S, as well as nitrogen oxides, depending on the type of animals and feed used at the feedlot (Feilberg et al., 2017; Koelsch et al., 2004). The cattle feedlots on the Mpumalanga Highveld are open, dry feedlots, meaning that animals are not kept in confined environments. However, at the Kanhym cattle feedlot, there is also a very large piggery. The pigs are housed in closed buildings and could also contribute to gaseous emissions. In Fig. 20, a simultaneous increase of H_2S, SO_2 and NO_2 is observed between 23:00 on 30 November and 02:00 on 1 December 2009. It was not expected to observe an increase in SO_2 in a feedlot plume, but this could be due to fractional oxidation of emitted H_2S during transport of the air mass. The

Fig. 19. Google Earth image of the Kanhym feedlot and piggery. The blue polygon indicates active feedlots, the green polygon shows inactive feedlots, the yellow polygons indicate the piggery, the purple polygon is a waste treatment dam, the pink polygons are silage production areas and the cyan polygon indicate a stagnant water body that has discoloured, likely due to manure runoff (a run-off path from the one end of the feedlot to the dam is clearly visible).

north-eastern interior of South Africa is in general characterised by relatively high O_3 concentrations (e.g. Laban et al., 2018), which will contribute to high levels of the hydroxyl radical ($OH^{\bullet}$) (albeit not characterised and quantified yet in South Africa) (Seinfeld and Pandis, 2006). Additionally, co-emission of SO_2 from combustion sources at the feedlot (e.g. heavy vehicles, refuse combustion and household combustion) could also have contributed to it being measured as a co-incidental species.

Fig. 21 clearly indicates air masses that had passed over the Kanhym and SIS feedlots. However, three power plants and one pyrometallurgical smelter lie within this FLEXPART footprint area. The timing of the co-incidental concentration peaks does not eliminate high stack emissions as a potential source, but it makes it very unlikely since it was observed late at night when low-level thermal inversion layers are present (Garstang et al., 1996; Gierens et al., 2018; Korhonen et al., 2014). Furthermore, the peak amplitudes were not indicative of a fresh coal-fired power station plume. Although the contribution from a coal-fired power station cannot be completely excluded, this plume was associated mainly with feedlot emissions.

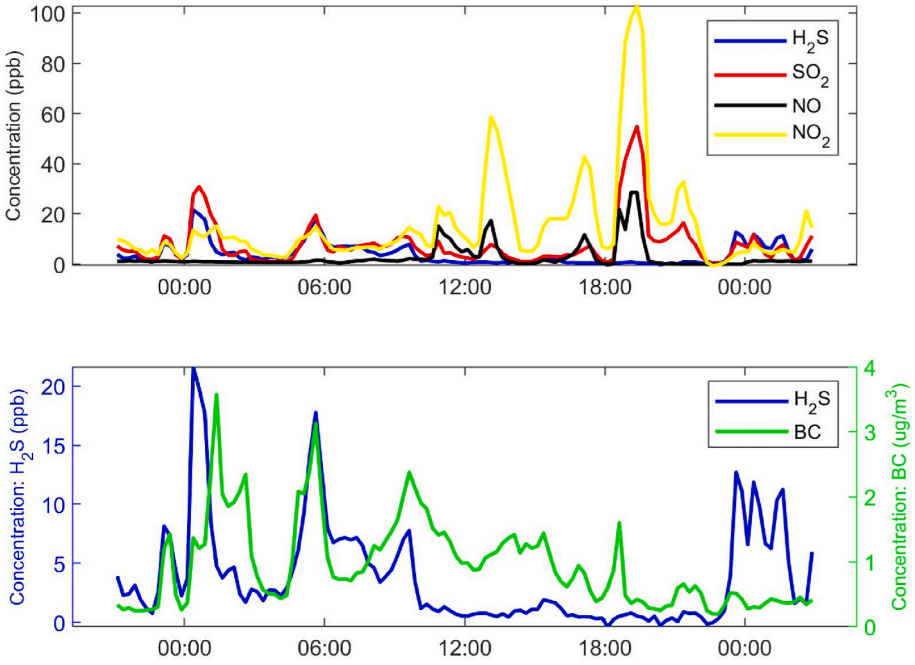

Fig. 20. 24hr ± 3hr time series concentration graphs of co-incidental increases of H_2S, SO_2 and NO_2 on the 30th of November 2009.

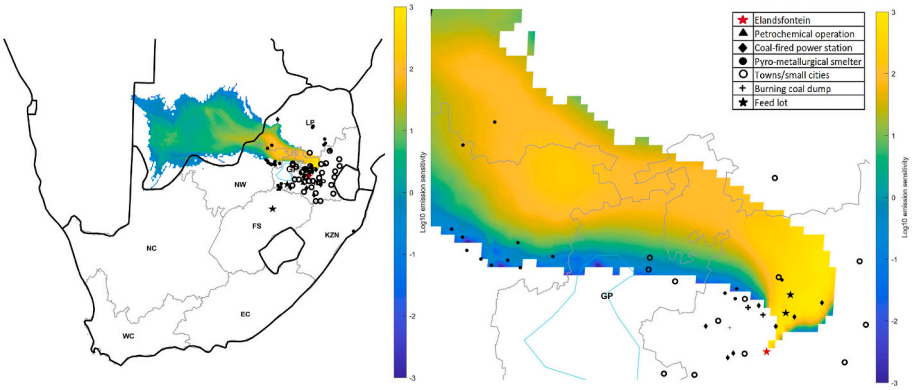

Fig. 21. Summed up FLEXPART emission sensitivities for the example co-incidental H_2S plume depicted in Fig. 21.

3.3.6. Burning coal dumps

Emissions from spontaneous combustion of coal (coal dumps/seams) on the Mpumalanga Highveld have recently been semi-quantified in a study where fire radiative power observations were used to determine these activities (Cogho et al., 2022). Coal mining is a prevalent activity in this region and a consequence is the exposure of coal to oxygen, which can cause spontaneous combustion of coal. It has been suggested that the spontaneous combustion of coal may have significant environmental impacts (Pone et al., 2007, Cogho et al., 2022), since the ineffective combustion of sulphur containing coal will emit H_2S (Sussman and Mulhern, 1964). The formation of H_2S from burning coal dumps could be from two possible reaction pathways (Reactions 1 and 2) (Sussman and Mulhern, 1964).

$$H_2SO_4 + FeS \rightarrow FeSO_4 + H_2S \quad (1)$$

$$C + 2SO_2 \rightarrow CS_2 + 4H_2O$$

$$CS_2 + 2H_2O \rightarrow 2H_2S + CO_2 \quad (2)$$

In Fig. 22, a simultaneous increase of H_2S, SO_2 and a slight increase in eBC is observed between 07:00 and 09:00 on the 20th of September 2010. These increases were unlikely to be from high stack emissions, due to the timing of the co-incidental peaks, as previously indicated (Garstang et al., 1996; Gierens et al., 2018; Korhonen et al., 2014). This co-incidental increase in H_2S, SO_2 and eBC are not necessarily indicative of the emissions of burning coal, as it is similar to the emissions of other low-level sources (e.g. urban and feedlot emissions). However, from inspection of the back-trajectory paths (Fig. 23), it is evident that the air masses passed directly over an actively burning coal field that was identified with the method presented by Beukes et al. (2018) and Cogho et al. (2022) (explained in Section 2.4).

In the Google Earth image presented in Fig. 24, a polygon indicating the area surrounded by the blue circle in Fig. 23 is presented. Historically the coal fields in the area were mined by using a room and pillar technique. This is an underground mining practice in which pillars of coal are left within a coal seam to provide support for the roof of the underground operation, while the coal surrounding the pillars are mined to form "rooms" (Bell et al., 2001; Pone et al., 2007). More recently, opencast mining operations to mine the left over "pillars", exposes the coal "pillars" to an influx of oxygen, which results in the spontaneous combustion of some of the coal (Bell et al., 2001; Pone et al., 2007). The combustion process can become self-sustaining in the presence of oxygen once the coal is burning hot enough and large quantities of coal is available, which makes containing these fires extremely difficult (Bell et al., 2001).

3.4. H_2S source contributions

Fig. 25 presents a simple bar plot of the H_2S source contributions to ambient H_2S concentrations in excess of the baseline (which was 2.7 ppb, when plume periods were excluded), conducted with the method introduced and discussed in Section 2.5. Co-incidental concentration peaks were allocated to eight different sources, namely the petrochemical operation near Secunda (indicated as "Petrochemical"), coal-fired power stations (indicated as "Powerstation"), pyrometallurgical smelters (indicated as "Pyrometallurgical), urban (not including the Jhb-Pta megacity), Jhb-Pta megacity, feedlots, burning coal dumps (indicated as "Coal dumps") and mixed.

It is evident from Fig. 25 that the largest contributor to ambient H_2S levels measured in excess of the baseline concentrations observed at Elandsfontein, were urban emissions (i.e. 34.6%). As previously stated, these urban emissions include all H_2S emissions associated with cities/towns/in- and semiformal settlements (excluding emissions from the Jhb-Pta megacity) e.g. household combustion, waste water treatment facilities, landfills, small industries, as well as traffic emissions, especially, from older diesel vehicles (Kourtidis et al., 2007; Sengupta, 2014; Colomer et al., 2012; Hac Ko et al., 2015). In the diurnal H_2S patterns (Fig. 25), bimodal peaks were identified in the early mornings and evenings, which were attributed to low-level emissions that can be trapped near the surface (Garstang et al., 1996; Gierens et al., 2018; Korhonen et al., 2014). Therefore, the afore-mentioned result, i.e. urban emissions having the largest contribution to H_2S measured at Elandsfontein, agrees with the deductions made from the seasonal and diurnal patterns. It should be noted, though, that the urban category may include some industrial emissions in rare cases, where night-time mixing brings high stack emissions down to the surface. It is also possible that a plume from a more distant point source that reached ground level the previous day would be observed during night-time at Elandsfontein.

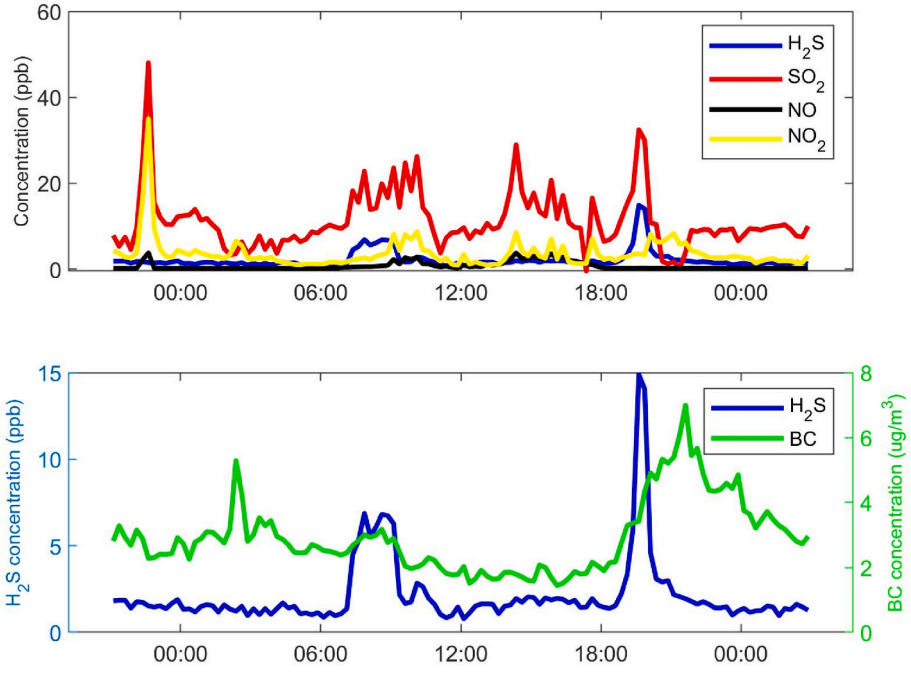

Fig. 22. 24hr ± 3hr *time series concentration graphs* of co-incidental increases of H_2S, SO_2, NO_2 and eBC on the 20th of September 2010.

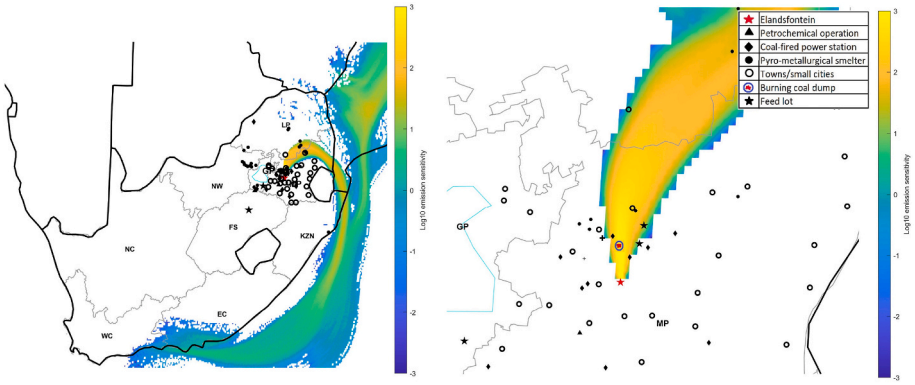

Fig. 23. Summed up FLEXPART emission sensitivities for the example co-incidental H_2S plume depicted in Fig. 22 as well as fire locations (red dots) identified with the method presented by Beukes et al. (2018).

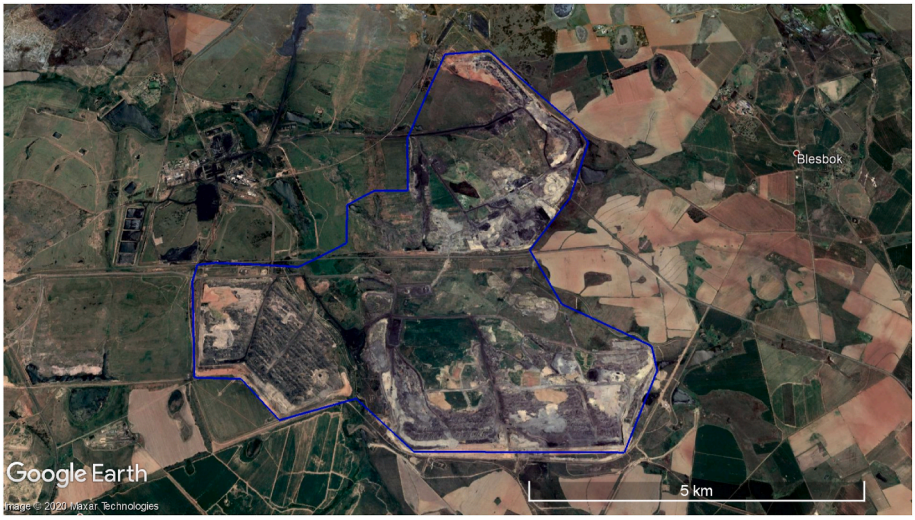

Fig. 24. Google Earth image of the area identified as a burning coal field in Fig. 23.

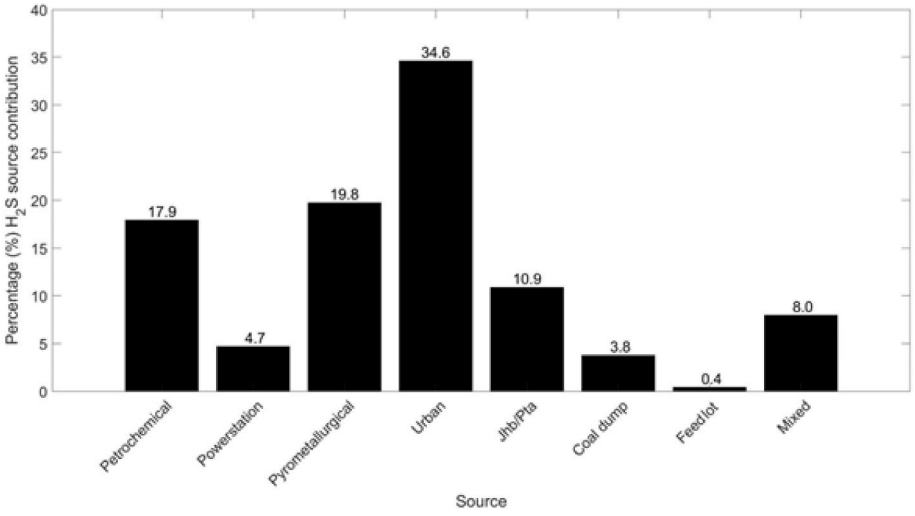

Fig. 25. Percentage source contributions in excess of the baseline concentrations for each of the identified sources as calculated with the method introduced in Section 2.5.

Thus, the contribution here is an upper limit value and deficiencies associated with this defined source group are acknowledged. However, it is still a good indication of H_2S emissions associated with urban areas.

It is well known that the petrochemical operation near Secunda emits H_2S, since the coal pyrolysis gasification process applied (Bunt and Waanders, 2008), suppresses the formation of SO_2 (the corresponding

oxidised gaseous species). Therefore, high contributions to ambient H_2S measured at Elandsfontein is expected. However, according to the receptor source quantification results presented in this study, i.e. contribution of 17.9% to the H_2S (Fig. 25) measured in excess of the baseline concentrations at Elandsfontein, it is evident that it is not the main contributor of H_2S measured in excess of the baseline at Elandsfontein. Chiloane et al. (2017) found that the pyrometallurgical smelters in the Middelburg/Witbank area contributed to H_2S measured at Elandsfontein, however, the factional contribution of this industry sector was not quantified in the aforementioned study. The results presented in this paper (Fig. 25) indicated that the pyrometallurgical smelters in the area contributed 19.8% to H_2S measured in excess of the baseline concentrations. The Jhb-Pta megacity was also indicated to be a significant contributor to H_2S measured in excess of the baseline concentrations at Elandsfontein, with a contribution of 10.9% (Fig. 25). Combined, the urban- and Jhb-Pta sources accounted for 45.5% of the H_2S in excess of the baseline.

Coal-fired power stations also contributed to the ambient H_2S measured in excess of the baseline concentrations at Elandsfontein, with a smaller, but not insignificant contribution of 4.7% (Fig. 25). It was not expected to measure H_2S in plumes originating from coal-fired power stations, since the combustion process requires oxidising conditions that favour the formation of SO_2 and not H_2S. However, two possible explanations for H_2S emission associated with coal-fired power stations was considered, i.e. use of low-NO_x burners (Engineering News, 2017; Shirai et al., 2012; Van der Merwe et al., 2017) and a non-ideal oxidative environment experienced during boiler start-ups (ESKOM, 2019). These are explained in greater detail in Section 3.4.5.b.

Burning coal dumps had a small, but not insignificant, contribution to ambient H_2S in excess of the baseline, contributing 3.8% to the total ambient H_2S measured at Elandsfontein. In relation to the relatively small number, size and sporadic activities of these burning coal dumps, they make a surprisingly large contribution to the ambient H_2S levels. Feedlots had the smallest individual contribution to the ambient H_2S measured in excess of baseline concentrations at Elandsfontein i.e. 0.4%. Three very large feedlots, each with $\geq$20 000 animals, could be identified as sources. These animals do not directly emit H_2S, but there are generally two sources at feedlots where H_2S is produced, i.e.: i) in waste runoff retention structures or treatment lagoons, and ii) accumulation of manure in pens and manure storage areas (Preece et al., 2018). In both of these locations, anaerobic wet conditions allow for the decomposition of manure to produce H_2S (Preece et al., 2018; Rubright et al., 2017). Additionally, anaerobic decomposition of silage feed could also serve as a small H_2S source, but, as far as the authors could determine, no studies have been conducted to assess this potential source. It is generally accepted that feedlots do not emit H_2S in very large quantities (Koelsch et al., 2004). Lastly, the co-incidental concentration peaks that were attributed to "Mixed" sources contributed approximately 8% of the H_2S measured in excess of the baseline concentrations at Elandsfontein.

In addition to the abovementioned source contributions, statistics of the ratios of baseline corrected H_2S concentrations divided by baseline corrected concentrations of the other species relevant to each source type is presented in Table 4. As previously stated, very little H_2S data is available for South Africa in the peer reviewed public domain. Therefore, such ratios can be used in future modelling studies as approximated emission factors to estimate H_2S, if only concentration(s) of other species are known. However, care should be taken when these ratios are used, since atmospheric conversion processes of the various species cited in Table 4 are influenced by plume age, methodological conditions (e.g., high stack emission mostly observed during certain times of the day on the South African Highveld) and ambient conditions (e.g., difference between daytime and night-oxidation processes).

4. Summary and conclusions

Ambient H_2S concentrations and sources were investigated in detail for the first time in southern Africa in this study. Measurements reveals that H_2S forms a considerable fraction (>20%) of the total gas phase sulphur burden over the industrial hub of South Africa. Consequently, it appears to be an important contributor also to the particulate sulphate in southern Africa, with implications to air quality and acid deposition in this region. Seasonal and diurnal patterns of the H_2S concentration at the Elandsfontein measurement site suggest that surface emissions are the predominant source of H_2S in the region.

A review of industrial and other anthropogenic activities in the Mpumalanga Highveld suggests a number of potential sources of H_2S in the region. Investigation into H_2S plumes in excess of the baseline concentrations indicates substantial contributions from most of these sources. Emissions from urban areas (excluding the Jhb-Pta megacity) were identified as the largest contributor, which accounted for 34.6% of the H_2S in excess of the baseline concentrations. In addition, the Jhb-Pta megacity contributed another 10.9%, which was a bit lower than the contribution from the petrochemical operation near Secunda (17.9%). Pyrometallurgical smelters, coal-fired power stations, burning coal dumps and large feedlots contributed approximately 19.8, 4.7, 3.8 and 0.4%, respectively. However, it should be noted that especially urban and megacity categories may contain contributions from surrounding industrial sources.

Table 4
Mean and median, as well as the 5th, 25th, 75th and 95th percentile concentration values of the calculated H_2S ratios.

Source	Ratio											
	H_2S/SO_2						H_2S/NO_2					
	Mean	**Median**	**5th**	**25th**	**75th**	**95th**	**Mean**	**Median**	**5th**	**25th**	**75th**	**95th**
Powerstaion	0.45	0.20	0.02	0.08	0.58	1.97	0.56	0.28	0.02	0.09	0.62	2.49
Petrochemical	1.22	0.94	0.13	0.57	1.49	2.85	0.88	0.79	0.12	0.49	1.14	1.96
Pyrometallurgical	0.76	0.68	0.20	0.42	0.96	1.50	1.50	1.16	0.20	0.58	2.20	3.49
Urban	1.55	0.59	0.15	0.39	0.93	3.50	1.46	0.87	0.18	0.47	1.76	4.12
Jhb/Pta	0.61	0.47	0.14	0.31	0.65	1.33	1.88	1.14	0.18	0.60	1.96	3.44
Coal dump	0.98	0.67	0.23	0.41	1.02	2.79	1.80	1.05	0.12	0.64	2.87	4.89
Feedlot	1.00	0.97	0.10	0.67	1.24	2.21	1.04	0.90	0.11	0.31	1.52	2.68
	H_2S/NO						**H_2S/eBC**					
	Mean	**Median**	**5th**	**25th**	**75th**	**95th**	**Mean**	**Median**	**5th**	**25th**	**75th**	**95th**
Powerstation	10.79	4.66	0.58	2.96	8.27	37.45	5.19	0.47	0.02	0.11	2.41	27.46
Petrochemical	7.76	2.53	0.16	0.90	5.70	40.20	34.63	18.18	2.90	8.34	42.82	98.19
Pyrometallurgical	35.46	10.15	0.46	3.62	35.88	154.94	7.17	4.90	1.04	3.01	7.85	25.71
Urban	24.06	8.55	0.40	2.51	26.70	94.45	14.76	6.95	1.27	3.20	13.49	55.86
Jhb/Pta	31.19	14.78	0.82	4.46	33.55	138.26	9.03	5.47	1.72	3.47	9.98	24.71
Coal dump	27.48	8.77	0.83	2.87	28.93	103.86	10.89	6.83	1.54	4.16	12.09	27.09
Feedlot	5.46	2.35	0.02	1.23	5.31	25.03	14.92	7.35	3.12	4.86	11.25	66.13

There are three limitations to the applied source apportioning method. Firstly, only H_2S contributions in excess of the baseline concentrations can be identified and quantified. Therefore, diffused, diluted and very small sources, which contribute to the baseline concentrations, were not apportioned. Secondly, the method partially depended on the investigators' understanding of local/regional sources, emission patterns of these sources (e.g., seasonal and diurnal patterns), regional meteorological patterns (e.g., boundary layer evolution) and atmospheric conversion processes (e.g., fresh and aged plume differences). Hence, the method should only be applied by investigators with intimate local and regional knowledge, and who understand the fundamental scientific principles. Thirdly, the method is quite time consuming to apply, since user input is required for the identification and allocation of each co-incidental H_2S peak. A future prospect would be to develop a machine learning algorithm, which can be trained to identify and allocate co-incidental peaks for any set of species for a specific measurement site. Notwithstanding these limitations, significant additional insight into source apportionment can be obtained with this method, as demonstrated here.

Currently the South African DEA is considering the formulation of regional specific H_2S ambient air quality standard limits. The results from this study should be used to inform this process. The combined contribution from urban regions (excluding Jhb-Pta megacity) and the Jhb-Pta megacity were 56.6% to H_2S concentrations in excess of the baseline in the Mpumalanga Highveld. This indicated that focus should foremost be on poverty alleviation, which will reduce household combustion of low grade coal in semi- and informal settlements, as well as matters controlled by local and municipal government e.g. uncontrolled refuse combustion, mismanaged sewage water facilities (for which South Africa is infamous at present, e.g. Tempelhoff, 2009) and poorly maintained diesel vehicles that are allowed to be used – all of which are likely sources to contribute to the observed emissions associated with urban emissions of H_2S. If the envisaged legislation is applied to only focus on large industrial point sources, it will likely reduce the occurrence of so-called "high H_2S" days (a day on which an 1-h average H_2S concentration exceeds 29 ppb), but possibly not reduce the overall ambient levels. Thirteen such "high H_2S" days were recorded at Elandsfontein during the two-year measurement period considered in this study, which were attributed to different sources. The proposed legislations should also take into consideration that the average baseline concentration measured during this 2-year sampling period was 2.7 ppb, which can be ascribed to diluted industrial- and background emissions from very diffused, diluted and very small sources that will not be influenced by legislation.

Authors' contributions

EC, JPB, PGvZ and VV were the main investigators in this study and wrote the manuscript. EC conducted this study as part of his PhD degree, as well as performed most of the experimental work and data processing. The project was led by JPB, PGvZ and VV, which were also study leaders of the PhD. LL and MJ assisted with sample collection and site maintenance. MK provided financial support for the measurements, while LL and MK also made conceptual contributions.

Declaration of competing interest

The authors declare that they have no known competing financial interests or personal relationships that could have appeared to influence the work reported in this paper.

Data availability

Data will be made available on request.

Acknowledgements

Financial support from the University of Helsinki, the Finnish Meteorological Institute and the European Aerosol Cloud Climate and Air Quality Interactions project (EUCAARI) (FP6 project, contract 34684), as well as logistical support from ESKOM and SASOL, are acknowledged. E. Cogho, who is a PhD candidate, also benefitted indirectly from financial support of the Department of Science and Innovation of South Africa, as part of the Biogeochemistry Research Infrastructure Platform (BIOGRIP) and also received limited funding from SASOL. The authors wish to acknowledge CSC – IT Center for Science, Finland, for computational resources.

Appendix A. Supplementary data

Supplementary data to this article can be found online at https://doi.org/10.1016/j.atmosenv.2023.120140.

References

AERONET, 2020. AERONET Aerosol Optical Data Display Interface. https://aeronet.gsfc.nasa.gov/cgi-bin/data_display_aod_v3?site=Elandsfontein&nachal=2&level=1&place_code=10. (Accessed 18 February 2020).

Air Resources Laboratory, 2014. National Oceanic and Atmospheric Administration (NOAA). https://www.ready.noaa.gov/gdas1.php. (Accessed 20 July 2019).

Aurela, M., Beukes, J.P., van Zyl, P.G., Vakkari, V., Teinilä, K., Saarikoski, S., Laakso, L., 2016. The composition of ambient and fresh biomass burning aerosols at a savannah site, South Africa. South Afr. J. Sci. 112, 1–8. https://doi.org/10.17159/sajs.2016/20150223.

Backman, J., Virkkula, A., Vakkari, V., Beukes, J.P., Van Zyl, P.G., Josipovic, M., Piketh, S., Tiitta, P., Chiloane, K., Petäjä, T., Kulmala, M., Laakso, L., 2014. Differences in aerosol absorption Ångström exponents between correction algorithms for a particle soot absorption photometer measured on the South African Highveld. Atmos. Meas. Tech. 7, 4285–4298. https://doi.org/10.5194/amt-7-4285-2014.

Balmer, M., 2007. Household coal use in an urban township in South Africa. J. Energy South Afr. 18, 27–32. https://doi.org/10.17159/2413-3051/2007/v18i3a3382.

Bates, M.N., Garrett, N., Crane, J., Balmes, J.R., 2013. Associations of ambient hydrogen sulfide exposure with self-reported asthma and asthma symptoms. Environ. Res. 122, 81–87. https://doi.org/10.1016/j.envres.2013.02.002.

Belaid, M., Falcon, R., Vainikka, P., 2014. Pulverized coal versus circulating fluidized-bed boilers Perspectives and challenges for South Africa. S. Afr. J. Chem. Eng. 19, 72–81. https://hdl.handle.net/10520/EJC167219.

Bell, F.G., Bullock, S.E.T., Hälbich, T.F.J., Lindsay, P., 2001. Environmental impacts associated with an abandoned mine in the Witbank Coalfield, South Africa. Int. J. Coal Geol. 45, 195–216. https://doi.org/10.1016/S0166-5162(00)00033-1.

Beukes, J.P., Venter, A.D., Josipovic, M., Van Zyl, P.G., Vakkari, V., Jaars, K., Dunn, M., Laakso, L., 2015. Automated Continuous Air Monitoring, Monitoring of Air Pollutants, p. 408.

Beukes, J.P., Du Preez, S.P., Van Zyl, P.G., Paktunc, D., Fabritius, T., Päätalo, M., Cramer, M., 2017. Review of Cr(VI) environmental practices in the chromite mining and smelting industry – Relevance to development of the Ring of Fire, Canada. Journal of Cleaner Production 165, 874–889. https://doi.org/10.1016/j.jclepro.2017.07.176.

Beukes, J.P., Van Zyl, P.G., Sifiev, M., Soares, J., Liebenberg-Enslin, H., Shackleton, N., Sunström, A.-M., 2018. The use of satellite observations of fire radiative power to estimate the availabilities (activity patterns) of pyrometallurgical smelters. J. S. Afr. Inst. Min. Metall 118, 619–624. https://doi.org/10.17159/2411-9717/2018/v118n6a9.

Bunt, J.R., Waanders, F.B., 2008. Identification of the reaction zones occurring in a commercial-scale Sasol-Lurgi FBDB gasifier. Fuel 87, 1814–1823. https://doi.org/10.1016/j.fuel.2007.11.012.

Chiloane, K.E., Beukes, J.P., van Zyl, P.G., Maritz, P., Vakkari, V., Josipovic, M., Venter, A.D., Jaars, K., Tiitta, P., Kulmala, M., Wiedensohler, A., Liousse, C., Mkhatshwa, G.V., Ramandh, A., Laakso, L., 2017. Spatial, temporal and source contribution assessments of black carbon over the northern interior of South Africa. Atmos. Chem. Phys. 17, 6177–6196. https://doi.org/10.5194/acp-17-6177-2017.

Cogho, E., Beukes, J.P., van Zyl, P.G., Vakkari, V., 2022. The use of fire radiative power observations to determine spontaneus combustion event activities associated with coal mining on the Mpumalanga Highveld. Clean Air J. 32 https://doi.org/10.17159/caj/2022/32/2.12145.

Collett, K.S., Piketh, S.J., Ross, K.E., 2010. An assessment of the atmospheric nitrogen budget on the South African Highveld. South Afr. J. Sci. 106 https://doi.org/10.4102/sajs.v106i5/6.220.

Colomer, F.L., Morató, H.E., Iglesias, E.M., 2012. Estimation of hydrogen sulfide emission rates at several wastewater treatment plants through experimental concentration measurements and dispersion modelling. J. Air. Waste. Manage. 62 (7), 758–766. https://doi.org/10.1080/10962247.2012.674008.

Conradie, E.H., Van Zyl, P.G., Pienaar, J.J., Beukes, J.P., Galy-Lacaux, C., Venter, A.D., Mkhatshwa, G.V., 2016. The chemical composition and fluxes of atmospheric wet

deposition at four sites in South Africa. Atmos. Environ. 146, 113–131. https://doi.org/10.1016/j.atmosenv.2016.07.033.
Di, Q., Wang, Y., Zanobetti, A., Wang, Y., Koutrakis, P., Choirat, C., Dominici, F., Schwartz, J.D., 2017. Air pollution and mortality in the medicare population. N. Engl. J. Med. 376, 2513–2522. https://doi.org/10.1056/NEJMoa1702747.
Delmas, R., Baudet, J., Servant, J., Baziard, Y., 1980. Emissions and concentrations of hydrogen sulfide in the air of the tropical forest of the Ivory Coast and of temperate regions in France. J. Geophys. 85, 148–227. https://doi.org/10.1029/JC085iC08p04468.
Department of Environmental Affairs, 2010. State of Air Report 2005. A Report on the State of Air in South Africa. Department of Environmental Affairs.
Du Preez, S.P., Beukes, J.P., Van Zyl, P.G., 2015. Cr(VI) Generation during flaring of CO-rich off-gass from closed ferrochromium submerged arc furnaces. Metall. Mater. Trans. 46, 1002–1010. https://doi.org/10.1007/s11663-014-0244-3.
Engelbrecht, J.P., Swanepoel, L., Chow, J.C., Watson, J.G., Egami, R.T., 2002. The comparison of source contributions from residential coal and low-smoke fuels, using CMB modeling, in South Africa. Environ. Sci. Pol. 5, 157–167. https://doi.org/10.1016/S1462-9011(02)00029-1.
ENGINEERING NEWS, 2017. Camden Power Station to Receive Last of 164 Burners. http://www.engineeringnews.co.za/article/camden-power-station-to-receive-last-of-164-burners-2017-01-27. (Accessed 18 February 2019).
ESKOM, 2019. Power Generation Overview. www.eskom.co.za/AboutElectricity/FactsFig.s/Documents/CO0002HowElecProducedCoalFiredRev11.pdf. (Accessed 22 February 2019).
Feilberg, A., Hansen, M.J., Liu, D., Nyord, T., 2017. Contribution of livestock H2S to total sulfur emissions in a region with intensive animal production. Nat. Commun. https://doi.org/10.1038/s41467-017-01016-2.
Garstang, M., Tyson, P.D., Swap, R., Edwards, M., Kållberg, P., Lindesay, J.A., 1996. Horizontal and vertical transport of air over southern Africa. J. Geophys. 101, 721–736. https://doi.org/10.1029/95JD00844.
Giannakaki, E., Pfülle, A., Korhonen, K., Mielonen, T., Laakso, L., Vakkari, V., Baars, H., Engelman, R., Beukes, J.P., Van Zyl, P.G., Josipovic, M., Tiitta, P., Chiloane, K., Piketh, S.J., Lihavainen, H., Lehtinen, K.E.J., Komppula, M., 2015. One year of Ramen lidar observations of free-tropospheric aerosol layers over South Africa. Atmos. Chem. Phys. 15, 5429–5442. https://doi.org/10.5194/acp-15-5429-2015.
Gierens, R.T., Laakso, L., Mogensen, D., Vakkari, V., Beukes, J.P., Van Zy, l P.G., Hakola, H., Guenther, A., Pienaar, J.J., Boy, M., 2004. Modelling new particle formation events in the South African savannah. South Afr. J. Sci. 110, 5–6. https://doi.org/10.1590/sajs.2014/20130108.
Gierens, R.T., Henriksson, S., Josipovic, M., Vakkari, V., Van Zyl, P.G., Beukes, J.P., Wood, C.R., O'Connor, E.J., 2018. Observing continental boundary-layer structure and evolution over the South African savannah using a ceilometer. Theor. Appl. Climatol. https://doi.org/10.1007/s00704-018-2484-7.
Hac Ko, J., Xu, Q., Jang, Y.-C., 2015. Emissions and control of hydrogen sulfide at landfills: a review. Crit. Rev. Environ. Sci. Technol. 45 (19), 2043–2083. https://doi.org/10.1080/10643389.2015.1010427.
Hinz, R., 2011. Hydrogen Sulphide in Rotorua, New Zealand: Personal Exposure Assessment and Health Effects. Massey University, Palmerston North, p. 166. MSc Dissertation.
Hyvärinen, A.P., Vakkari, V., Laakso, L., Hooda, R.K., Sharma, V.P., Panwar, T.S., Beukes, J.P., van Zyl, P.G., Josipovic, M., Garland, R.M., Andreae, M.O., Pöschl, U., Petzold, A., 2013. Correction for a measurement artifact of the Multi-Angle Absorption Photometer (MAAP) at high black carbon mass concentration levels. Atmos. Meas. Tech. 6, 81–90. https://doi.org/10.5194/amt-6-81-2013.
Jaars, K., Vestenius, M., van Zyl, P.G., Beukes, J.P., Hellén, H., Vakkari, V., Venter, M., Josipovic, M., Hakola, H., 2018. Receptor modelling and risk assessment of volatile organic compounds measured at a regional background site in South Africa. Atmos. Environ. 172, 133–148. https://doi.org/10.1016/j.atmosenv.2017.10.047.
Koelsch, R.K., Woodbury, B.L., Stenberg, D.E., Miller, D.N., Schulte, D.D., 2004. Total reduced sulfur concentration in vicinity of beef cattle feedlots. In: Biological Systems Engineering: Papers and Publications, vol. 4. https://digitalcommons.unl.edu/biosysengfacpub/4. (Accessed 19 February 2020).
Korhonen, K., Giannakaki, E., Mielonen, T., Pfuller, A., Laakso, L., Vakkari, V., Baars, H., Engelman, R., Beukes, J.P., Van Zyl, P.G., Ramandh, A., Ntsangwane, L., Josipovic, M., Tiitta, P., Fourie, G., Ngwana, I., Chiloane, K., Komppula, M., 2014. Atmospheric boundary layer top height in South Africa: measurements with lidar and radiosonde compared to three atmospheric models. Atmos. Chem. Phys. 14, 4264–4278. https://doi.org/10.5194/acp-14-4263-2014.
Kourtidis, K., Kelesis, A., Petrakakis, M., 2007. Hydrogen sulphide (H2S) in urban ambient air. Atmos. Environ. 42, 7476–7482. https://doi.org/10.1016/j.atmosenv.2008.05.066.
Kuik, F., Lauer, A., Beukes, J.P., van Zyl, P.G., Josipovic, M., Vakkari, V., Laakso, L., Feig, G.T., 2015. The anthropogenic contribution to atmospheric black carbon concentrations in southern Africa: a WRF-Chem modeling study. Atmos. Chem. Phys. 15, 8809–8830. https://doi.org/10.5194/acp-15-8809-2015.
Kulmala, M., Asmi, A., Lappalainen, H.K., Baltensperger, U., Brenguier, J.L., Facchini, M. C., Hansson, H.C., Hov, Ø., O'Dowd, C.D., Pöschl, U., Wiedensohler, A., Boers, R., Boucher, O., de Leeuw, G., Denier van der Gon, H.A.C., Feichter, J., Krejci, R., Laj, P., Lihavainen, H., Lohmann, U., McFiggans, G., Mentel, T., Pilinis, C., Riipinen, I., Schulz, M., Stohl, A., Swietlicki, E., Vignati, E., Alves, C., Amann, M., Ammann, M., Arabas, S., Artaxo, P., Baars, H., Beddows, D.C.S., Bergström, R., Beukes, J.P., Bilde, M., Burkhart, J.F., Canonaco, F., Clegg, S.L., Coe, H., Crumeyrolle, S., D'Anna, B., Decesari, S., Gilardoni, S., Fischer, M., Fjaeraa, A.M., Fountoukis, C., George, C., Gomes, L., Halloran, P., Hamburger, T., Harrison, R.M., Herrmann, H., Hoffmann, T., Hoose, C., Hu, M., Hyvärinen, A., Hõrrak, U., Iinuma, Y., Iversen, T., Josipovic, M., Kanakidou, M., Kiendler-Scharr, A., Kirkevåg, A., Kiss, G., Klimont, Z., Kolmonen, P., Komppula, M., Kristjánsson, J.-E., Laakso, L., Laaksonen, A., Labonnote, L., Lanz, V.A., Lehtinen, K.E.J., Rizzo, L.V., Makkonen, R., Manninen, H. E., McMeeking, G., Merikanto, J., Minikin, A., Mirme, S., Morgan, W.T., Nemitz, E., O'Donnell, D., Panwar, T.S., Pawlowska, H., Petzold, A., Pienaar, J.J., Pio, C., Plass-Duelmer, C., Prévôt, A.S.H., Pryor, S., Reddington, C.L., Roberts, G., Rosenfeld, D., Schwarz, J., Seland, Ø., Sellegri, K., Shen, X.J., Shiraiwa, M., Siebert, H., Sierau, B., Simpson, D., Sun, J.Y., Topping, D., Tunved, P., Vaattovaara, P., Vakkari, V., Veefkind, J.P., Visschedijk, A., Vuollekoski, H., Vuolo, R., Wehner, B., Wildt, J., Woodward, S., Worsnop, D.R., van Zadelhoff, G.-J., Zardini, A.A., Zhang, K., van Zyl, P.G., Kerminen, V.-M., S Carslaw, K., Pandis, S.N., 2011. General overview: European Integrated project on Aerosol Cloud Climate and Air Quality interactions (EUCAARI) – integrating aerosol research from nano to global scales. Atmos. Chem. Phys. 11, 13061–13143. https://doi.org/10.5194/acp-11-13061-2011.
Laakso, L., Vakkari, V., Virkkula, A., Laakso, H., Backman, J., Kulmala, M., Beukes, J.P., van Zyl, P.G., Tiitta, P., Josipovic, M., Pienaar, J.J., Chiloane, K., Gilardoni, S., Vignati, E., Wiedensohler, A., Tuch, T., Birmili, W., Piketh, S., Collett, K., Fourie, G. D., Komppula, M., Lihavainen, H., de Leeuw, G., Kerminen, V.M., 2012. South African EUCAARI measurements: seasonal variation of trace gases and aerosol optical properties. Atmos. Chem. Phys. 12, 1847–1864. https://doi.org/10.5194/acp-12-1847-2012.
Laban, T.L., Van Zyl, P.G., Beukes, J.P., Vakkari, V., Jaars, K., Borduas-Dedekind, N., Josipovic, M., Thompson, A.M., Kulmala, M., Laakso, L., 2018. Seasonal influences on surface ozone variability in continental South Africa and implications for air quality. Atmos. Chem. Phys. 18, 15491–15514. https://doi.org/10.5194/acp-18-15491-2018.
Langerman, K.E., Pauw, C.J., Smith, H.J., Piketh, S.J., 2018. Moving households to cleaner energy through air quality offsets. In: International Conference on the Domestic Use of Energy (DUE), Cape Town, pp. 1–8. https://doi.org/10.23919/DUE.2018.8384405.
Lourens, A.S.M., Beukes, J.P., Van Zyl, P.G., Fourie, G.D., Burger, J.W., Pienaar, J.J., Read, C.E., Jordaan, J.H.L., 2011. Spatial and Temporal assessment of Gaseous Pollutants in the Mpumalanga Highveld of South Africa. S Afr J Sci. 107 (1/2) https://doi.org/10.4102/sajs.v107i1/2.269. Art. #269, 8 pages.
Lourens, A.S.M., Butler, T.M., Beukes, J.P., Van Zyl, P.G., Beirle, S., Wagner, T.K., Heue, K.-P., Pienaar, J.J., Fourie, G.D., Lawrence, M.G., 2012. Re-evaluating the NO_2 hotspot over the South African Highveld. South Afr. J. Sci. 108 https://doi.org/10.4102/sajs.v108i11/12.1146.
Lourens, A.S.M., Butler, T.M., Beukes, J.P., van Zyl, P.G., Fourie, G.D., Lawrence, M.G., 2016. Investigating atmospheric photochemistry in the Johannesburg-Pretoria megacity using a box model. South Afr. J. Sci. 112, 1–11. https://doi.org/10.17159/sajs.2016/2015-0169.
Maenhaut, W., Salma, I., Cafmeyer, J., Annegarn, H.J., Andreae, M.O., 1996. Regional atmospheric aerosol composition and sources in the eastern Transvaal, South Africa, and impact of biomass burning. J. Geophys. 101, 23631–23650. https://doi.org/10.1029/95JD02930.
Makonese, T., Masekameni, D.M., Annegarn, H.J., Forbes, P.B.C., 2015. Influence of fire-ignition methods and stove ventilation rates on gaseous and particle emissions from residential coal braziers. J. Energy South Afr. 26, 16–28. http://www.scielo.org.za/scielo.php?script=sci_arttext&pid=S1021-447X2015000400002&lng=en&nrm=iso. ISSN 2413-3051.
Mathee, A., von Schirnding, Y.E.R., 2003. Air quality and health in greater Johannesburg. In: McGranahan, G., Murray, F. (Eds.), Air Pollution and Health in Developing Countries. Earthscan Publications, London, pp. 206–219.
Mbonane, T.P., Masekameni, D., Mokoatle, C., Kasangana, K.K., 2018. A review paper on traditional fuel use, indoor air pollution, and Respiratory diseases: lessons for South Africa. In: 2018 International Conference on the Domestic Use of Energy, Cape Town, pp. 1–7. https://doi.org/10.23919/DUE.2018.8384406.
Mphepya, J.N., Galy-Lacaux, C., Lacaux, J.P., Held, G., Pienaar, J.J., 2006. Precipitation chemistry and wet deposition in Kruger national park, South Africa. J. Atmos. Chem. 53, 169–183. https://doi.org/10.1007/s10874-005-9005-7.
Mphepya, J.N., Pienaar, J.J., Galy-Lacaux, C., Held, G., Turner, C.R., 2004. Precipitation chemistry in semi-arid areas of southern Africa: a case study of a rural and an industrial site. J. Atmos. Chem. 47, 1–24. https://doi.org/10.1023/B:JOCH.0000012240.09119.c4.
Mucina, L., Rutherford, M.C., 2006. The Vegetation of South Africa, Lesotho and Swaziland. Strelitzia 19. South African National Biodiversity Institute, Pretoria.
Nieminen, T., Kerminen, V.-M., Petäjä, T., Aalto, P.P., Arshinov, M., Asmi, E., Baltensperger, U., Beddows, D.C.S., Beukes, J.P., Collins, D., Ding, A., Harrison, R. M., Henzing, B., Hooda, R., Hu, M., Hõrrak, U., Kivekäs, N., Komsaare, K., Krejci, R., Kristensson, A., Laakso, L., Laaksonen, A., Leaitch, W.R., Lihavainen, H., Mihalopoulos, N., Németh, Z., Nie, W., O'Dowd, C., Salma, I., Sellegri, K., Svenningsson, B., Swietlicki, E., Tunved, P., Ulevicius, V., Vakkari, V., Vana, M., Wiedensohler, A., Wu, Z., Virtanen, A., Kulmala, M., 2018. Global analysis of continental boundary layer new particle formation based on long-term measurements. Atmos. Chem. Phys. 18, 14737–14756. https://doi.org/10.5194/acp-18-14737-2018.
Petzold, A., Ogren, J.A., Fiebig, M., Laj, P., Li, S.M., Baltensperger, U., Holzer-Popp, T., Kinne, S., Pappalardo, G., Sugimoto, N., Wehrli, C., Wiedensohler, A., Zhang, X.Y., 2013. Recommendations for reporting black carbon measurements. Atmos. Chem. Phys. 13, 8365–8379. https://doi.org/10.5194/acp-13-8365-2013.
Piketh, S.J., Van Nierop, M., Rautenbach, C., Walton, N., Ross, K., Holmes, S., Richards, T., 2005. Rustenburg Local Municipality Air Quality Management Plan, Palace Consulting Engineers Ltd. Republic of South Africa.
Pisso, I., Sollum, E., Grythe, H., Kristiansen, N.I., Cassiani, M., Eckhardt, S., Arnold, D., Morton, D., Thompson, R.L., Groot Zwaaftink, C.D., Evangeliou, N., Sodemann, H.,

Haimberger, L., Henne, S., Brunner, D., Burkhart, J.F., Fouilloux, A., Brioude, J., Philip, A., Siebert, P., Stohl, A., 2019. The Langrangian particle dispersian model FLEXPART version 10.4. Geosci. Model Dev 12, 4955–4997. https://doi.org/10.5194/gmd-12-4955-2019.

Preece, S.L.M., Casey, K.D., Auvermann, B.W., 2018. Hydrogen Sulfide Emissions from Open/Dry-Lot-Cattle-Feeding Operations. Texas A & M Agrilife Extension. https://agrilifeextension.tamu.edu/library/ranching/hydrogen-sulfide-emissions-from-open-dry-lot-cattle-feeding-operations/. (Accessed 19 February 2020).

Pretorius, I., Piketh, S.J., Burger, R., Neomagus, H., 2015. A perspective on South African coal fired power station emissions. J. Energy South Afr. 26, 27–40. http://www.scielo.org.za/scielo.php?script=sci_arttext&pid=S1021-447X2015000300004&lng=en&nrm=iso. ISSN 2413-3051.

Pone, J.D.N., Hein, K.A.A., Stratcher, G.B., Annegarn, H.J., Finkleman, R.B., Blake, D.R., McCormack, J.K., Schroeder, P., 2007. The spontaneous combustion of coal and its by-products in the Witbank and Sasolburg coalfields of South Africa. Int. J. Coal Geol. 72, 124–140. https://doi.org/10.1016/j.coal.2007.01.001.

Rubright, S.L.M., Pearce, L.L., Peterson, J., 2017. Environmental toxicology of hydrogen sulfide. Nitric Oxide 71, 1–13. https://doi.org/10.1016/j.niox.2017.09.011.

Seinfeld, J.H., Pandis, S.N., 2006. Atmospheric Chemistry and Physics: from Air Pollution to Climate Change, second ed. John Wiley & Sons, Inc, p. 219.

Sengupta, A., 2014. Preliminary Hydrogen Sulfide Emission Factors and Emission Models for Wastewater Treatment Plant Headworks. University of New Orleans Theses and Dissertations, p. 1829. https://scholarworks.uno.edu/td/1829.

Scorgie, Y., 2012. Air Quality Management Planning in South Africa. PhD Thesis. University of Johannesburg, p. 295.

Shirai, H., Ikeda, M., Aramaki, H., 2012. Characteristics of hydrogen sulphide formation in pulverized coal combustion. Fuel 114, 114–119. https://doi.org/10.1016/j.fuel.2012.03.028.

Seibert, P., Frank, A., 2004. Source-receptor matrix calculation with a Lagrangian particle dispersion model in backward mode. Atmos. Chem. Phys. 4, 51–63. https://doi.org/10.5194/acp-4-51-2004.

Skrtic, L., 2006. Hydrogen Sulfide, Oil and Gas, and People's Health. MSc dissertation, University of California, Berkeley, p. 77p.

Slatt, B.J., Natusch, D.F.S., Prospero, J.M., Savoie, D.L., 1967. Hydrogen sulphide in the atmosphere of the northern equatorial Atlantic Ocean and its relation to the global sulfur cycle. Atmos. Environ. 12, 981–991. https://doi.org/10.1016/0004-6981(78)90342-6.

Stern, D.I., 2006. Reversal of the trend in global anthropogenic sulfur emissions. Global Environ. Change 16, 207–220. https://doi.org/10.1016/j.gloenvcha.2006.01.001.

Stohl, A., 1998. Computation, accuracy and application of trajectories – a review and bibliography. Atmos. Environ. 32, 947–966. https://doi.org/10.1016/S1352-2310(97)00457-3.

Stohl, A., Forster, C., Frank, A., Seibert, P., Wotawa, G., 2005. Technical note: the Lagrangian particle dispersion model FLEXPART version 6.2. Atmos. Chem. Phys. 5, 2461–2474. https://doi.org/10.5194/acp-5-2461-2005.

Sussman, V.H., Mulhern, J.J., 1964. Air pollution from coal refuse disposal areas. J. Air Pollut. Control Assoc. 14 (7), 279–284. https://doi.org/10.1080/00022470.1964.10468282.

Tempelhoff, J.W.N., 2009. Civil society and sanitation hydropolitics: a case study of South Africa's Vaal River Barrage. Phys. Chem. Earth, Parts A/B/C 34 (3), 164–175. https://doi.org/10.1016/j.pce.2008.06.006.

Tiitta, P., Vakkari, V., Croteau, P., Beukes, J.P., van Zyl, P.G., Josipovic, M., Venter, A.D., Jaars, K., Pienaar, J.J., Ng, N.L., Canagaratna, M.R., Jayne, J.T., Kerminen, V.M., Kokkola, H., Kulmala, M., Laaksonen, A., Worsnop, D.R., Laakso, L., 2014. Chemical composition, main sources and temporal variability of PM1 aerosols in southern African grassland. Atmos. Chem. Phys. 14, 1909–1927. https://doi.org/10.5194/acp-14-1909-2014.

Vakkari, V., Tiitta, P., Jaars, K., Croteau, P., Beukes, J.P., Josipovic, M., Kerminen, V.M., Kulmala, M., Venter, A.D., van Zyl, P.G., 2015. Reevaluating the contribution of sulfuric acid and the origin of organic compounds in atmospheric nanoparticle growth. Geophys. Res. Lett. 42 https://doi.org/10.1002/2015GL066459.

Van der Merwe, C., Sukdeo, P., Peta, S., Smit, D., 2017. Eskom Low NOx burner combustion simulation experience. In: 2017 ANSYS Engineering Simulation Conference. https://www.researchgate.net/publication/329443440_ESKOM_Low_NOx_burner_combustion_simulation_experience_-_A_Low_NOx_burner_design_case_study.

Van Zyl, P.G., Beukes, J.P., du Toit, G., Mabaso, D., Hendriks, J., Vakkari, V., Tiitta, P., Pienaar, J.J., Kulmala, M., Laakso, L., 2014. Assessment of atmospheric trace metals in the western Bushveld Igneous Complex, South Africa. South Afr. J. Sci. 110, 1–10. https://doi.org/10.1590/sajs.2014/20130280.

Venter, A.D., Beukes, J.P., Van Zyl, P.G., Josipovic, M., Jaars, K., Vakkari, V., 2016. Regional atmospheric Cr(VI) pollution from the bushveld complex, South Africa, atmos. Pollut. Res. 7, 762–767. https://doi.org/10.1016/j.apr.2016.03.009.

Venter, A.D., van Zyl, P.G., Beukes, J.P., Josipovic, M., Hendriks, J., Vakkari, V., Laakso, L., 2017. Atmospheric trace metals measured at a regional background site (Welgegund) in South Africa. Atmos. Chem. Phys. 17, 4251–4263. https://doi.org/10.5194/acp-17-4251-2017.

Venter, A.D., van Zyl, P.G., Beukes, J.P., Swartz, J.-S., Josipovic, M., Vakkari, V., Laakso, L., Kulmala, M., 2018. Size resolved characterisation of inorganic ionic species in atmospheric aerosols at a regional background site on the South African Highveld Air Quality. J. Atmos. Chem. 72, 285–304. https://doi.org/10.1007/s10874-018-9378-z.

Venter, M., Beukes, J.P., van Zyl, P.G., Vakkari, V., Vikkula, A., Josipovic, M., Kulmala, M., Laakso, L., 2020. Six-year observations of aerosol optical properties at a southern African grassland savannah site. Atmos. Environ. 230 https://doi.org/10.1016/j.atmosenv.2020.117477.

Wiedensohler, A., Birmili, W., Nowak, A., Sonntag, A., Weinhold, K., Merkel, M., Wehner, B., Tuch, T., Pfeifer, S., Fiebig, M., Fjäraa, A.M., Asmi, E., Sellegri, K., Depuy, R., Venzac, H., Villani, P., Laj, P., Aalto, P., Ogren, J.A., Swietlicki, E., Williams, P., Roldin, P., Quincey, P., Hüglin, C., Fierz-Schmidhauser, R., Gysel, M., Weingartner, E., Riccobono, F., Santos, S., Grüning, C., Faloon, K., Beddows, D., Harrison, R., Monahan, C., Jennings, S.G., O'Dowd, C.D., Marinoni, A., Horn, H.-G., Keck, L., Jiang, J., Scheckman, J., McMurry, P.H., Deng, Z., Zhao, C.S., Moerman, M., Henzing, B., de Leeuw, G., Löschau, G., Bastian, S., 2012. Mobility particle size spectrometers: harmonization of technical standards and data structure to facilitate high quality long-term observations of atmospheric particle number size distributions. Atmos. Meas. Tech. 5, 657–685. https://doi.org/10.5194/amt-5-657-2012.

Xiao, Z., Laplante, A.R., 2004. Characterizing and recovering the platinum group minerals-a review. Mner. Eng. 17, 961–979. https://doi.org/10.1016/j.mineng.2004.04.001.